

# Characterizing the load profile in power grids by Koopman mode decomposition of interconnected dynamics

Ali Tavasoli<sup>1</sup>, Behnaz Moradijamei<sup>2</sup>, Heman Shakeri<sup>1\*</sup>

<sup>1</sup>School of Data Science, University of Virginia, Charlottesville, VA, USA

<sup>2</sup>Department of Mathematics & Statistics, James Madison University, Harrisonburg, VA, USA

\*Corresponding author's email: hs9hd@virginia.edu

## Abstract

Electricity load forecasting is crucial for effectively managing and optimizing power grids. Over the past few decades, various statistical and deep learning approaches have been used to develop load forecasting models. This paper presents an interpretable machine learning approach that identifies load dynamics using data-driven methods within an operator-theoretic framework. We represent the load data using the Koopman operator, which is inherent to the underlying dynamics. By computing the corresponding eigenfunctions, we decompose the load dynamics into coherent spatiotemporal patterns that are the most robust features of the dynamics. Each pattern evolves independently according to its single frequency, making its predictability based on linear dynamics. We emphasize that the load dynamics are constructed based on coherent spatiotemporal patterns that are intrinsic to the dynamics and are capable of encoding rich dynamical features at multiple time scales. These features are related to complex interactions over interconnected power grids and different exogenous effects. To implement the Koopman operator approach more efficiently, we cluster the load data using a modern kernel-based clustering approach and identify power stations with similar load patterns, particularly those with synchronized dynamics. We evaluate our approach using a large-scale dataset from a renewable electric power system within the continental European electricity system and show that the Koopman-based approach outperforms a deep learning (LSTM) architecture in terms of accuracy and computational efficiency. The code for this paper has been deposited in a GitHub repository, which can be accessed at the following address [github.com/Shakeri-Lab/Power-Grids](https://github.com/Shakeri-Lab/Power-Grids)

*Keywords:* Power grids, load forecasting, Koopman operator, spectral analysis, spatiotemporal patterns, clustering.

## 1 Introduction

There are two types of load forecasting approaches: physics-based and data-driven modeling. Physics-based models are used to understand the different aspects that collectively determine the spatiotemporal multilayer dynamics of power systems, resulting from the interaction between node dynamics and topology. This interaction leads to phenomena such as synchronization and cascade effects [Filatrella et al., 2008; Motter et al., 2013; Nardelli et al., 2014]. However, physics-based approaches may be less reliable due to assumptions about properties and environmental parameters. Therefore, data-driven approaches are becoming increasingly popular due to the rapid development of sensor technologies and data mining techniques. These methods are being used to reduce uncertainty and provide more robust load forecasts [Saric et al., 2021; Wang et al., 2022; Hu et al., 2022a]. Long-term forecasts (over three years) of peak electricity demand are crucial for capacity planning and maintenance scheduling [Hyndman and Fan, 2010]. However, recently, very short-term (below one day), short-term (a day to two weeks), and medium-term (two weeks to three years) forecasts have received more attention for secure operation and planning of power systems, as well as control and scheduling, and commercial issues in energy markets [Amjady, 2001; Song et al., 2005; Taylor and McSharry, 2007; Taylor, 2008; Fan and Hyndman, 2012; Charlton and Singleton, 2014; Goude et al., 2014].

Data-driven load forecasting methods can be broadly classified into two categories: conventional statistical methods and artificial intelligence methods. Conventional statistical models use time series analysis to extract statistical information from data and make predictions about future data points by assuming that future data is related to historically observed data. Examples of linear statistical models include ordinary regression models [Weron, 2006], auto-regressive moving average model (ARMA) [Pappas et al., 2010], Autoregressive integrated moving average model (ARIMA) [Chodakowska et al., 2021], and exponential smoothing [Taylor and McSharry, 2007]. For nonlinear problems in energy prediction and evaluation, methods such as random forest (RF) [Dudek, 2015], support Vector Regression (SVR) [Chen et al., 2017], gradient boost [Patnaik et al., 2021], Gaussian process [Shepero et al., 2018], or fuzzy systems [Efendi et al., 2015] are used. However, due to their greater flexibility in constructing forecasting models in the presence of features such as nonlinearity, high volatility, and uncertainty of load profiles, artificial intelligence models generally outperform conventional statistical models in terms of forecasting accuracy [Deb et al., 2017; Bianchi et al., 2017; Nti et al., 2020]. Therefore, artificial intelligence methods are increasingly used for load forecasting, while conventional statistical models are still used in certain applications.

The early machine learning (ML) methods for load forecasting were based on Support Vector Machines (SVM) [Chen et al., 2004] and basic (shallow) Neural Networks (NNs) [Tsekouras et al., 2006; Sözen et al., 2007; Geem and Roper, 2009; Ardakani and Ardehali, 2014]. Later on, more sophisticated techniques such as Deep NNs (DNNs) [Din and Marnerides, 2017], Convolutional NNs (CNNs) [Voß et al., 2018], and Long Short-Term Memory (LSTM) [Marino et al., 2016; Kong et al., 2019] emerged. However, deep architectures are prone to overfitting, which hinders their forecasting accuracy. To overcome this limitation, researchers have proposed elaborate structures that use different details and units hierarchically to process data at different levels [Shi et al., 2018; Zhang et al., 2018; Afrasiabi et al., 2020; Dudek and Pełka, 2021; Yin et al., 2023].

In modern machine learning frameworks, interpretable and generalizable models are promoted for studying physical systems using architectures such as Sparse Identification of Nonlinear Dynamics (SINDy) [Brunton et al., 2016; Brunton and Kutz, 2019]. However, most neural network approaches lack interpretability, making them difficult to analyze and interpret [Brunton and Kutz, 2022]. Moreover, while these networks are effective at interpolating and memorizing training data, they often struggle with extrapolation and generalization beyond the training data. This limitation hinders their application in physical and engineering systems, where models extracted from limited training data must be valid beyond the training range for prediction, optimization, and control purposes. Additionally, in power grid applications, where nonlinear interactions in large interconnected systems can have arbitrary size and structure, computationally tractable approaches that carefully capture the underlying dynamical features are needed.

To address the challenges in modeling physical systems, we adopt an operator theoretic framework to study load data—where the data is understood by exploring the underlying dynamics manifold. By using the Koopman operator, we can represent the underlying dynamics in terms of intrinsic coordinates that efficiently capture the most predictable features of the load dynamics. This allows us to approximate the nonlinear dynamics with a linear one but in an  $\infty$ -dimensional space. By studying the spectral properties of the Koopman operator, we can decompose the load dynamics into a set of independent spatiotemporal modes that effectively encode the complex interactions in interconnected power grids. These modes can be used to achieve a minimum-order realization of the large-scale power grids that provides a globally linear description over the entire data domain. We use a cluster-based Koopman forecasting method to better realize Koopman modes for power stations with similar properties. This method employs a modern kernel approach, namely the PHATE [Moon et al., 2019], which captures both local and global nonlinear data structure using an information-geometric distance between data points. The PHATE effectively reveals the stations with synchronized dynamics, allowing us to cluster them together for more accurate forecasting.

The rest of the paper is organized as follows. First, Section 2 reviews the relevant literature. Then, in Section 3, the Koopman operator is introduced, followed by a discussion of the data-driven approach to identifying it in Section 4. Section 5 describes the clustering approach used. Next, our results are presented in Section 6. Finally, concluding remarks are provided in Section 7.

## 2 Literature review

**Physics-informed approaches:** Recent studies have explored the use of physics-informed methods to create load forecasting models that are both interpretable and generalizable. As highlighted by [Tartakovsky and Tipireddy, 2019; Stock et al., 2022], these methods are particularly relevant for load forecasting, where large interconnected subsystems operate under various stochastic and exogenous factors. To effectively model such systems and achieve reduced dynamic representations, sparsity-promoting approaches like SYNDy are essential [Brunton et al., 2016]. These approaches preserve the physical plausibility of the original model but often require significant physics-derived information to identify the appropriate basis, which belongs to a pre-selected family. Furthermore, they lead to nonlinear models that hinder the use of linear approaches for subsequent analysis and design purposes.

**Koopman operator approach:** The significance of the Koopman operator is its connection with a different class of physically-interpretable data-driven approaches that use a natural basis for the learning process by extracting and decomposing the intrinsic manifold of the data. This approach produces intrinsic coordinates, also known as coherent patterns of dynamics, that are equivalent to the eigenfunctions of the Koopman operator in the geometric study of dynamical systems [Mezić, 2005]. In the field of signal processing, the Koopman operator can be viewed as an extension of Fourier analysis, replacing predefined frequency bases with intrinsic spectra of the underlying dynamical system and temporal patterns with (intrinsic) spatiotemporal patterns [Lange et al., 2021]. The Koopman operator’s eigenfunctions also recover a coherent temporal pattern with an associated timescale, making it ideal for studying multiscale systems [Giannakis, 2019; Marrouch et al., 2020; Froyland et al., 2021]. Various settings have been proposed to present the Koopman approach, including Dynamic Mode Decomposition (DMD) [Tu et al., 2014], Extended DMD (EDMD) [Williams et al., 2015], graph DMD [Fujii and Kawahara, 2019], Hankel matrix analysis [Arbabi and Mezić, 2017], spectral moment estimation [Korda et al., 2020], Galerkin [Thiede et al., 2019], and deep learning [Lusch et al., 2018]. However, we use an ergodic theory framework, first presented in [Mezić, 2005] and later extended based on kernel operators and delay coordinates in [Giannakis, 2019; Das and Giannakis, 2019; Klus et al., 2020; Das et al., 2021], to extract spatiotemporal load dynamics patterns. This approach relies on integral kernel operators’ property to approximate the Laplace-Beltrami operator eigenfunctions, which recover the geometry of the nonlinear manifold comprised by the data [Coifman and Lafon, 2006a]. The Laplace-Beltrami basis addresses traditional approaches’ limitations, such as Principal Component Analysis (PCA), in capturing the intermittent features of signals [Giannakis and Majda, 2012, 2013].

Recent research has utilized the Dynamic Mode Decomposition (DMD) technique for short-term electric load forecasting and has demonstrated improved accuracy and stability compared to traditional methods [Rowley et al., 2009; Schmid, 2010]. Additionally, DMD can adapt to various exogenous factors such as time, weather, seasonality, economics, and social activities without explicitly incorporating them into the forecasting model [Mohan et al., 2018; Kong et al., 2020; Dylewsky et al., 2022]. Moreover, DMD’s performance is independent of complex training procedures, feature selection, and parameter tuning, and it requires less computational and processing resources compared to single-structure and ensemble models for load forecasting [Mohan et al., 2018]. However, DMD inherits the limitations of singular value decomposition and cannot effectively capture complex nonlinear and transient phenomena [Schmid, 2022; Brunton et al., 2022]. To address these issues, we use the Koopman operator to incorporate nonlinear observables that are better suited to the nonlinear and non-stationary load patterns.

**Spatiotemporal forecasting:** In matching distributed renewable energy with urban energy demand at large scales, understanding spatiotemporal energy profiles is crucial [Mikkola and Lund, 2014]. To predict future changes for demand-side management, high-resolution temporal patterns must be realized, while increasing spatial resolution enables regional energy planning and capturing the spatial dynamics of energy demand drivers. Regional and local energy grids are interconnected with national and continental networks, making high resolution necessary everywhere to capture multiscale effects [Eggimann et al., 2019]. Recent studies on spatiotemporal load forecasting have employed LSTM deep learning methods [Peng et al., 2021; Zhu et al., 2022]. However, as discussed earlier, our work departs from deep learning approaches and presents a physically-interpretable data-driven approach that identifies load dynamics in an operator theoretic framework. Moreover, since the Koopman approach utilizes a more explicit basis for learning, it provides more

stability to the learned dynamical system compared to recurrent neural networks such as LSTM [Das et al., 2023]. Additionally, our approach offers computational efficiency through the Galerkin approach [Thiede et al., 2019], which does not require rigorous training phases and optimal parameter selections as required by deep learning approaches. Furthermore, our model extracts multiscale spatiotemporal modes where each temporal mode scales with a frequency of the load dynamics and the corresponding spatial mode describes different stations’ energy patterns at that scale. We observe that studying various spatial modes at multiple scales enables the identification of different energy consumption behaviors, providing important insights for decision makers [Niu et al., 2021]. The spatiotemporal patterns obtained from Koopman eigenfunctions are intrinsic to the dynamics, providing additional advantages to our approach.

**Clustering:** Clustering of demand profiles based on load data has been found effective for understanding local demand characteristics on different urban scales [Voulis et al., 2018]. Recently, there has been a growing interest in using low-dimensional embedding techniques to enhance data-driven approaches’ flexibility, intuition, and interpretability for exploring energy consumption patterns [Niu et al., 2021; Peng et al., 2021]. Nonlinear embedding techniques such as diffusion maps [Coifman and Lafon, 2006a], which preserve both global and local data relative structures, are superior to conventional linear dimensionality reduction approaches like PCA [Moon and Stirling, 2000]. We employ PHATE, a method optimized for two- or three-dimensional visualization, based on the potential of heat diffusion for affinity-based transition embedding [Moon et al., 2019]. PHATE allows for clustering based on the intrinsic structure of the load data and has improved properties compared to suboptimal approaches like t-SNE [van der Maaten and Hinton, 2008] and PCA, addressing concerns about sensitivity to noise and scrambled global structure of the data [Moon et al., 2019]. In this paper, we apply PHATE to a technological subsystem prototype and explore its power for detecting distinct energy patterns. We use a different variant of the original approach in [Moon et al., 2019], which involves using variable bandwidth kernels [Berry and Harlim, 2016] to construct the data graph with a more accurate realization of local data points’ similarities and interactions. The bandwidth is adapted based on the local data structure, resulting in improved geometric description of the data set.

**Spectral analysis in power grids:** Conventional methods such as Fourier analysis [Zhong and Tam, 2015], wavelet analysis [Li et al., 2017], or PCA [Rydin Gorjão et al., 2020] are frequently used to describe the characteristics of load profiles in the time domain [Zhong and Tam, 2012]. However, these methods impose extrinsic conditions on the dynamical system and may fail to capture frequencies across multiple scales, leading to inaccurate representations of the underlying system [Lange et al., 2021]. Furthermore, the accuracy of these methods and their advanced relatives like Dynamic Mode Decomposition (DMD) [Schmid, 2010] is limited to linear regions of the underlying state space, making them unsuitable for nonlinear data manifolds [Giannakis and Majda, 2012]. They also provide little information about the chaotic parts of the dynamics and the continuous part of the system spectrum, which are crucial to understanding power grid dynamics [Yu et al., 2003; Halekotte et al., 2021]. To address these challenges, Koopman eigenfunctions give rise to temporal patterns, each recovering a timescale  $2\pi/\omega$ , that are connected with a Nonlinear Laplacian Spectral Analysis (NLSA) [Giannakis and Majda, 2012] through eigenfunctions of the Laplace–Beltrami operator [Coifman and Lafon, 2006a] that recovers the geometry of the data manifold [Giannakis, 2019]. Obtained temporal patterns are specifically highly coherent with predictable temporal evolution intrinsic to the dynamical system—markedly different from that of the eigenfunctions of covariance operators approximated by conventional approaches.

**Exogenous effects:** Many load forecasting methods rely on exogenous data to increase their accuracy, but this data is often unavailable for the forecasted period. As a result, creating additional models to forecast exogenous effects becomes necessary. For example, in [Taylor, 2008], a weather forecast approach was proposed to improve short-term load forecasting using methods such as ARIMA and exponential smoothing. However, using a secondary forecasting module has drawbacks, as it can lead to significant errors affecting the primary forecasting task. Additionally, it is difficult to select key factors as input variables to build an electricity load forecasting model due to the limited impact of environmental factors such as temperature on the electricity load of industrial enterprises [Hu et al., 2022b]. Furthermore, the complexity of the forecast architecture increases with a secondary forecasting unit, which limits the numerical efficiency and interpretability of the final model. Existing literature on load forecasting takes a casual approach to consider



seasonality, based on either the calendar month or some meteorological parameter, which can be inconsistent and inaccurate, especially during transition periods, leading to high forecasting errors [Sharma and Jain, 2022]. The Koopman operator extends to systems with input and nonautonomous systems in a skew product dynamics setting [Marrouch et al., 2020], where Koopman eigenfunctions encode different dynamical features of system inputs. In the load forecasting application, Koopman eigenfunctions recover various input features, and their corresponding Dirichlet energy values are used to prioritize different encoded features, as we demonstrate in this paper.

### 3 Koopman operator

The Koopman approach considers the available data set as observables of a dynamical system with state space  $\mathcal{X}$  and flow map  $\Phi^t : \mathcal{X} \mapsto \mathcal{X}$ , where  $t \in \mathbb{R}$  denotes time. The system’s state at time  $t$  is given by  $x_t = \Phi^t(x)$ , where  $x \in \mathcal{X}$ . The recorded signal at  $d$  sensors is viewed as an observation function  $F : \mathcal{X} \mapsto \mathbb{R}^d$ . The dynamical system  $(\mathcal{X}, \Phi^t)$  possesses ergodic measures; hence there exists a probability measure  $\mu$  on  $\mathcal{X}$ , invariant under the flow map  $\Phi^t$ , such that for every integrable function  $f : \mathcal{X} \mapsto \mathbb{C}$ , the time average  $\bar{f}$  of  $f$  converges to the expectation value  $\bar{f} = \int_{\mathcal{X}} f d\mu$ . Associated with the triplet  $(\mathcal{X}, \Phi^t, \mu)$ , we consider a Hilbert space  $\mathcal{H} = L^2(\mathcal{X}, \mu)$  of square-integrable observables with respect to  $\mu$ .

The group of unitary Koopman operators  $U^t : \mathcal{H} \mapsto \mathcal{H}$  governs the evolution of observables under  $\Phi^t$ . That means given  $f \in \mathcal{H}$ ,  $g = U^t f$  is defined as the observable satisfying  $g(x) = f(\Phi^t(x))$  for  $x \in \mathcal{X}$ . An observable  $\psi_j \in \mathcal{H}$  is a Koopman eigenfunction if it satisfies the eigenvalue equation

$$U^t \psi_j = e^{i\omega_j t} \psi_j \quad (1)$$

for all  $t \in \mathbb{R}$ . The eigenfrequency  $\omega_j$  is a real-valued frequency associated with the eigenfunction  $\psi_j$ . Therefore, in measure-preserving dynamical systems, the Koopman eigenvalues remain on the unit circle in the complex plane, and the corresponding eigenfunctions evolve periodically under the dynamics. This is the key to the predictability of coherent patterns of dynamics. The Koopman eigenvalues and eigenfunctions appear as complex-conjugate pairs, and the Koopman eigenfunctions that correspond to different eigenfrequencies are orthogonal in the Hilbert space  $\mathcal{H}$ . Let  $\mathcal{D}$  be the space of Koopman eigenfunctions that is invariant under  $U^t$ , and is the closure of the span of  $\psi_j$ . Every  $f \in \mathcal{D}$  can be decomposed as  $f = \sum_j \hat{f}_j \psi_j$ , where  $\hat{f}_j = \langle f, \psi_j \rangle$  is the inner product in  $\mathcal{H}$ . The norm in  $\mathcal{D}$  is denoted by  $\| \cdot \|$ . Moreover, the dynamical evolution of  $f$  can be computed in a closed form via

$$U^t f = \sum_j \hat{f}_j e^{i\omega_j t} \psi_j \quad (2)$$

For every continuous flow  $\Phi^t$ , the family of operators  $U^t$  has a generator  $V$ , which is a skew-adjoint operator, defined as

$$V f := \lim_{t \rightarrow 0} \frac{1}{t} (U^t f - f), \quad f \in D(V) \subset L^2(\mathcal{X}, \mu) \quad (3)$$

Operators  $U^t$  and  $V$  share the same eigenfunctions,

$$V \psi_j = i\omega_j \psi_j \quad (4)$$

For ergodic systems, all eigenvalues of  $V$  are simple.

## 4 The data-driven approach

### 4.1 Kernel operators and delay coordinates

Kernel methods have a long-standing history in machine learning [Hofmann et al., 2008], with established applications in detecting nonlinear data manifolds and order reduction [Coifman and Lafon, 2006a]. Recently, researchers have studied dynamics-dependent kernels in the context of dynamical systems [Berry and Sauer, 2016], with a particular focus on delay coordinate space. In this setting, kernel operators have demonstrated an impressive ability in capturing complex nonlinear phenomena [Giannakis, 2015].

Given a collection of  $N$  samples  $F(x_1), \dots, F(x_N)$ , organized in a time-ordered manner, where each  $F(x_i) \in \mathbb{R}^d$ . The value of  $x_n$  is determined by the function  $\Phi^{n\Delta t}(x_0)$ , where  $\Delta t$  is the interval at which the data is sampled. A delay coordinate map is constructed from  $F$  by embedding  $\mathcal{X}$  in a manifold in  $\mathbb{R}^{Qd}$  as

$$F_Q(x) = (F(x), F(\Phi^{-\Delta t}x), \dots, F(\Phi^{-(Q-1)\Delta t}(x))) \quad (5)$$

where  $Q$  (an integer) is the number of delays. Next, a kernel function  $k_Q : \mathcal{X} \times \mathcal{X} \mapsto \mathbb{R}_+$  is defined to measure the similarity of points in  $\mathcal{X}$  based on the observation function  $F_Q$ . In this work, we use the radial Gaussian kernel with variable bandwidth defined as:

$$k_Q(x, x') = \exp\left(-\frac{\|F_Q(x) - F_Q(x')\|^2}{\epsilon}\right) = \exp\left(-\frac{d_Q^2(x, x')}{\epsilon}\right) \quad (6)$$

where  $\epsilon$  is a positive bandwidth parameter that can vary based on the available data density in  $\mathcal{X}$ . In this work, we use a class of variable bandwidth kernels, also known as self-tuning kernels, introduced in [Berry and Harlim, 2016].

Associated with the square-integrable kernel  $k_Q$  is a compact integral operator,

$$K_Q f(x) := \int_{\mathcal{X}} k_Q(x, y) f(y) d\mu(y) \quad (7)$$

Then a Markov kernel is constructed by normalizing  $K_Q$ ,

$$P_Q f := \frac{\tilde{K}_Q f}{\tilde{K}_Q 1_{\mathcal{X}}} \quad (8)$$

where  $\tilde{K}f = K_Q(\frac{f}{K_Q 1_{\mathcal{X}}})$  and  $1_{\mathcal{X}}$  is the indicator function for the set  $\mathcal{X}$ .

As  $Q$  approaches infinity, the kernel integral operator  $P_Q$  commutes with  $U^t$ , as shown in [Das and Giannakis, 2019]. Commuting operators have a common eigenspace, which allows us to compute eigenfunctions of  $U^t$  through expansions in the basis obtained from  $P_Q$ . Compactness of  $P_Q$  makes a wide variety of data-driven tools available for approximation of integral operators.

## 4.2 Galerkin approximation of Koopman spectra

Solving for Koopman eigenvalues is a numerically ill-posed problem, as the eigenvalues of its generator,  $V$ , are dense on the imaginary axis in ergodic measure-preserving systems. This property adversely affects the stability of numerical approximations of Koopman eigenvalues and eigenfunctions. To address this challenge, finding the eigenvalues of  $V$  is replaced by approximating them through a regularized operator  $L_{\theta}$  with a small amount  $\theta$  of judiciously constructed diffusion added for regularization [Giannakis, 2019; Das and Giannakis, 2019]. Eigenfunctions of the Koopman operator are sought in a Sobolev subspace  $\mathcal{H}^2 \subset \mathcal{H}$  [Das and Giannakis, 2019], on which  $V$  is a bounded operator. Based on the standard Galerkin approach, the regularized Koopman eigenvalue problem is to find  $\gamma \in \mathbb{C}$  and  $z \in \mathcal{H}^2$ , such that for every  $f \in \mathcal{H}$  the following weak formulation holds:

$$\langle z, L_{\theta} f \rangle = \gamma \langle f, z \rangle, \quad L_{\theta} = V - \theta \Delta \quad (9)$$

where the operator  $\Delta$  is defined based on the eigenfunctions of the Laplace-Beltrami operator [Giannakis, 2019; Das and Giannakis, 2019]. In (9),  $\gamma$  and  $z$  are weak eigenvalues and eigenfunctions of  $L_{\theta}$ , and  $f$  is a test function. The role of the diffusion term is to penalize the eigenfunctions of  $V$  with large values of a Dirichlet energy functional, denoted by  $E(f) = \frac{\langle f, \Delta f \rangle}{\|f\|^2}$ . This energy functional measures the roughness of functions in the function space  $\mathcal{H}$ . This process leads to projecting the dynamics onto the smoothest possible set of Koopman eigenfunctions. To solve the Galerkin problem (9), we use the eigenfunctions  $\varphi_j$  of the kernel operator  $P_Q$  described in Section 4.1 as a basis. While the regularized operator  $L_{\theta}$  and the generator  $V$  share the same eigenfunctions, the eigenvalues of  $L_{\theta}$  are parameterized as  $\gamma_{\theta} = i\omega - \theta\eta$  where  $i\omega$  is an eigenvalue of  $V$  and  $\eta$  an eigenvalue of  $\Delta$ .

### 4.3 Data-driven Koopman eigenfunctions on sampled data

To put the above approach in a numerical setting, we arrange the load data as  $x_k = x(k\tau)$  where  $k = 1 : N$ , and  $\tau$  is the sampling interval. Each  $x_k \in \mathbb{R}^d$  represents a vector of load data at  $d$  spatial points, measured at time  $t = k\tau$ . The Markov kernel operator defines an orthonormal basis for the Koopman eigenfunctions, based on the data sampled along the orbit. The action of the kernel operator  $K_Q$  is approximated through a matrix  $K$  with the elements given as

$$K_{ij} = k_Q(x_i, x_j) = \exp\left(-\frac{d_Q^2(x_i, x_j)}{\epsilon}\right),$$

$$d_Q^2(x_i, x_j) = \frac{1}{Q} \sum_{k=0}^{Q-1} \|x_{i-k} - x_{j-k}\|^2$$
(10)

The normalized Markov kernel  $P_Q$  is approximated through the elements of the matrix  $P$  as

$$P_{ij} = \frac{K_{ij}}{(\sum_{k=1}^N K_{ik} q_k^{-1/2}) q_j^{1/2}}, \quad q_i = \sum_{k=1}^N K_{ik}$$
(11)

We obtain an approximation of the eigenvalues  $\lambda_j$  and eigenfunctions  $\varphi_j$  of the Markov kernel operator by solving the algebraic eigenvalue problem for  $P$ ,

$$P\varphi_j = \lambda_j \varphi_j$$
(12)

The matrix  $P$  provides an approximation of the ergodic average operation of  $P_Q$ , which is the fundamental concept behind kernel analog forecasting [Alexander and Giannakis, 2020]. To reduce the computational burden for large sample numbers  $N$ , we can sparsify  $P$  by selecting a cutoff value  $k_{nn} \ll N$  and setting all but the largest  $k_{nn}$  elements in each row of  $K$  to zero and symmetrizing the resulting sparse matrix.

The matrix  $P$  is a Markov matrix with real eigenvalues ordered as  $1 = \lambda_1 > \lambda_2 \geq \lambda_3 \geq \dots$ , and real eigenvectors  $\varphi_j$  that are mutually orthogonal in  $\mathbb{R}^N$ . Note that the first eigenvector corresponding to  $\lambda_1 = 1$  is the constant eigenvector  $\varphi_1 = (1, \dots, 1)^T \in \mathbb{R}^N$ , which has zero Dirichlet energy. One key feature of  $P_Q$  is that as  $Q \rightarrow \infty$ , it commutes (and hence has common invariant subspaces) with the Koopman operator  $U^t$ . Therefore, Koopman eigenfunctions can be approximated by a linear combination of kernel operator eigenfunctions:

$$\psi_i = \sum_{j=1}^l c_{ji} \varphi_j, \quad i = 1, \dots, l$$
(13)

where  $\psi_i \in \mathbb{R}^N$  denotes the  $i$ -th eigenfunction of  $U^t$  sampled at  $N$  data points. Hence,  $l \leq N$  first eigenfunctions of the kernel operator are used to approximate the Koopman eigenfunctions.

The matrix  $c_{l \times l} = [c_{ij}]$  is computed using a data-driven Galerkin approach [Thiede et al., 2019], in which the weak formulation (9) is approximated by the following matrix generalized eigenvalue problem:

$$A\hat{c} = \gamma B\hat{c}$$
(14)

where

$$A_{ij} = \langle \varphi_i, V\phi_j \rangle - \theta \langle \varphi_i, \Delta\phi_j \rangle$$

$$B_{ij} = \langle \varphi_i, \phi_j \rangle$$

$$\phi_i = \frac{\varphi_i}{\eta_i} \quad \eta_i = \frac{1}{\epsilon} (\lambda_i^{-1} - 1)$$
(15)

for  $i, j = 1, \dots, l$ . Each column of matrix  $c$  corresponds to a solution of  $\hat{c}$  in (14). Solutions  $(\gamma_i, \psi_i)$  are placed in order of increasing Dirichlet energy, calculated for each eigenfunction  $\psi_i$  as

$$E(\psi_i) = \frac{\langle \psi_i, \Delta\psi_i \rangle}{\|\psi_i\|^2}$$
(16)

The Dirichlet energy provides a measure of the spatial variability, or roughness, of functions on  $\mathcal{X}$ . A highly oscillatory eigenfunction in  $\mathcal{X}$  will have a large Dirichlet energy, whereas  $E(\psi_i)$  will be small if  $\psi_i$  is

spatially smooth. Therefore, unlike many existing approaches that require a library of functions to construct Koopman invariant subspaces, the kernel and delay coordinates approaches provide a data-driven basis for the Koopman eigenfunctions. This basis is optimal and dynamics-dependent, as it approximates the Laplace-Beltrami operator eigenfunctions [Giannakis, 2019; Das and Giannakis, 2019], which recovers the geometry of the nonlinear manifold on which data is collected [Coifman and Lafon, 2006a]. The Koopman eigenfunctions corresponding to nontrivial eigenvalues form complex-conjugate pairs with equal Dirichlet energies. The trivial eigenvalue ( $\lambda = 1$ ) has a constant eigenfunction over  $\mathcal{X}$  with zero Dirichlet energy.

We use the approach established in [Berry and Harlim, 2016] to achieve a variable bandwidth kernel where the bandwidth parameter is adaptively adjusted to be inversely proportional to the sampling density:

$$\epsilon = \epsilon(x_i, x_j) \propto \frac{1}{\rho^\alpha(x_i)\rho^\alpha(x_j)}, \quad \alpha \in \mathbb{R}^+ \quad (17)$$

where the sampling density function  $\rho(\cdot)$  and the constant  $\alpha$  are computed based on a kernel density estimation approach. The adaptive mechanism increases the bandwidth when the sampling density is small, and it decreases the bandwidth at regions where data is dense. Algorithm 1 provides a pseudocode for approximating the Koopman eigenfunctions.

#### 4.4 Spatiotemporal load reconstruction

We reconstruct the load data based on the temporal and spatial patterns of the dynamics. Initially, the projections of the observable variable  $F$  onto the Koopman eigenfunctions  $\psi_k$  are calculated as  $A_k(t) = \langle \psi_k, F \circ \Phi^t \rangle$ . This is numerically evaluated as shown in [Giannakis et al., 2018] using the equation:

$$A_k(q\tau) = \frac{1}{N} \sum_{n=1}^N \psi_{nk}^* x_{n-q}, \quad (18)$$

where the Koopman eigenfunctions are represented as  $\psi_k = (\psi_{1k}, \dots, \psi_{Nk})^T$ . The vector  $A_k(0)$  is called the  $k$ -th Koopman mode associated with the observable  $F$  [Mezić, 2005]. The spatial patterns generated by the Koopman eigenfunctions are derived from the elements of  $A_k$ . The spatiotemporal patterns related to the pair  $(\psi_k, A_k)$  are given by

$$x_n^{(k)} = \frac{1}{Q'} \sum_{q=0}^{Q'-1} A_k(q\tau) \psi_{(n+q,k)}, \quad Q' = \min\{Q, N - 1 - n\}, \quad 1 \leq n \leq N \quad (19)$$

where  $x_n^{(k)}$  is the contribution of the  $k$ -th Koopman eigenfunction to the reconstruction of  $x_n = x(n\tau)$ . To obtain a real-valued load reconstruction, the sum  $x_n^{(k)} + x_n^{(k+1)}$  is required since Koopman eigenfunctions form complex-conjugate pairs  $(\psi_k, \psi_{k+1})$ . As shown in equation (19), a reconstruction at time  $n\tau$  is a superposition of  $Q$  snapshots. This is a consequence of the time-lagged embedding and differs from a standard PCA analysis [Giannakis et al., 2018].

#### 4.5 Nystrom extension of Koopman eigenfunctions

As explained in Section 4.3, we use the original approach developed in [Giannakis, 2019; Das and Giannakis, 2019] to obtain the Koopman eigenfunctions that are sampled at the data points  $X_s = \{x_1, \dots, x_N\}$ . However, to evaluate the Koopman eigenfunctions at out-of-sample points, we utilize the Nystrom extension approach to extend the Koopman eigenfunctions to  $x \in \mathcal{X}/X_s$  in this work. To achieve this, we apply the Nystrom approach to extend the eigenfunctions  $\varphi_k$  of the Markov kernel operator first. Then, we use equation (13) for out-of-sample evaluation of Koopman eigenfunctions. Our approach is based on the method established in [Coifman and Lafon, 2006b].

Assuming that the Markov integral operator  $P_Q$  described in Section 4.1 has the kernel  $p_Q : \mathcal{X} \times \mathcal{X} \mapsto \mathbb{R}_+$ , the Nystrom extension method is employed to solve the eigenfunction of integral equations in the following form:

$$\int p_Q(x, y) \varphi(y) \nu(y) dy = \lambda \varphi(x) \quad (20)$$

---

**Algorithm 1** Approximating Koopman eigenfunctions from load data.

---

- Input
    - Time series  $\{x_k\}$ ,  $x_k \in \mathbb{R}^d$ , of the load sampled at  $d$  power stations every  $\tau$  time units
    - Parameter: Number of delays  $Q$
    - Parameter: Number of retained nearest neighbors  $k_{nn}$
    - Parameter: Number of Markov kernel eigenfunctions  $l \leq N$  used in Galerkin approximation
    - Koopman regularization parameter  $\theta \geq 0$
    - Number of Koopman eigenfunctions  $l' \leq l$  to be computed
  - Output
    - Koopman eigenvalues  $\gamma_1, \dots, \gamma_{l'}$  with  $\gamma_k \in \mathbb{C}$
    - Koopman eigenfrequencies  $\omega_1, \dots, \omega_{l'}$  with  $\omega_k \in \mathbb{R}$
    - Koopman eigenfunctions,  $\psi_1, \dots, \psi_{l'}$  with  $\psi_k \in \mathbb{C}^N$
  - Steps
    - 1: Compute the  $N \times N$  pairwise distances  $d_Q(x_i, x_j)$  using (10)
    - 2: For each  $i$  only retain the  $k_{nn}$  smallest values of  $d_Q(x_i, x_j)$  and consider the set  $\mathcal{N}_{k_{nn}}(x_i) = \{x_j | x_j \text{ in the } k_{nn} \text{ neighbourhood of } x_i\}$
    - 3: Symmetrize  $d_Q(x_i, x_j)$  by augmenting the list of retained distances for given  $i$  if  $x_i \in \mathcal{N}_{k_{nn}}(x_j)$  but  $x_j \notin \mathcal{N}_{k_{nn}}(x_i)$
    - 4: Determine the optimal bandwidth function  $\epsilon = \epsilon(x_i, x_j)$  using the procedure described in [Berry and Harlim, 2016]
    - 5: Form the  $N \times N$  matrix  $K$  in (10)
    - 6: Compute the  $N \times N$  sparse matrix  $P$  in (11)
    - 7: Compute the  $l$  largest eigenvalues  $\lambda_k$  of  $P$  and the corresponding kernel eigenfunctions  $\psi_k$
    - 8: Form the  $l \times l$  Galerkin approximation matrices  $A$  and  $B$  in (15)
    - 9: Solve the generalized eigenvalue problem (14) and obtain  $c_k$  as the  $k$ -th column of the matrix  $c_{l \times l}$  and the corresponding  $\gamma_k$  for  $k = 1, \dots, l$
    - 10: Compute Koopman eigenfunctions  $\psi_k$  for  $k = 1, \dots, l'$  using (13)
    - 11: Compute the Dirichlet energy  $E(\psi_k)$  of each eigenfunction using (16)
    - 12: Order the pairs  $(\gamma_k, \psi_k)$  in order of increasing Dirichlet energies
    - 13: Compute eigenfrequencies  $\omega_k = \text{Im}(\gamma_k)$
-

where  $\nu$  represents the underlying probability density function,  $\varphi(x)$  denotes the eigenfunction, and  $p_Q(x, y)$  signifies the similarity between  $x$  and  $y$ .

We consider the data  $X_s = \{x_1, x_2, \dots, x_N\}$ , sampled from the manifold  $\mathcal{X}$ , as  $N$  landmark points at which the eigenfunction  $\varphi$  is sampled. Using the Nystrom method, for any given point  $x \in \mathcal{X}$ , we obtain

$$\frac{1}{N} \sum_{i=1}^N p_Q(x, x_i) \hat{\varphi}(x_i) = \lambda \hat{\varphi}(x) \quad (21)$$

where  $\hat{\varphi}(x)$  is an approximation to the true  $\varphi(x)$ . Equation (21) cannot be solved directly, as  $\hat{\varphi}(x)$  and  $\lambda$  are both unknown. Let  $P$  denote the similarity matrix between the landmark points, with  $P_{ij} = p_Q(x_i, x_j)$ . By substituting  $x$  with  $x_i$  in Equation (21) and expressing it in matrix form, we obtain

$$P \hat{\varphi}_k = N \hat{\lambda}_k \hat{\varphi}_k, \quad k = 1, \dots, N \quad (22)$$

The solution of the eigenvalue problem (22) gives the eigenpair  $(\hat{\lambda}_k, \hat{\varphi}_k)$ , where  $\hat{\varphi}_k$  is the vector sampling  $\hat{\varphi}_k(x)$  at data points. To approximate the  $i$ -th eigenfunction at an unsampled point  $x$ , we use the following equation

$$\hat{\varphi}_i(x) = \frac{1}{N \hat{\lambda}_i} \sum_{j=1}^N p_Q(x, x_j) \hat{\varphi}_i(x_j) \quad (23)$$

The Koopman eigenfunctions are correspondingly evaluated by (13).

## 4.6 Forecasting by Koopman eigenfunctions

The work presented in [Giannakis, 2019; Das and Giannakis, 2019] proposes using (2) to predict observables in the Koopman invariant subspaces. However, real-world applications face two major challenges. First, while the regular part of the dynamics, e.g., the periodic and quasiperiodic dynamics, is associated with the discrete spectra and has a corresponding Koopman invariant subspace that fully describes its evolution, the irregular dynamics associated with the continuous spectra, e.g. the chaotic and mixing dynamics, have no corresponding Koopman invariant subspaces [Mezić, 2005]. As a result, some eigenfunctions recovered by the kernel and delay coordinates approaches are not exact Koopman eigenfunctions, rather, they are  *$\epsilon$ -approximate eigenfunctions* that satisfy (1) with a bound  $\epsilon$  controlled by the length of the delay-embedding window [Giannakis, 2021]. In particular, if  $z$  is an  $\epsilon$ -approximate eigenfunction, then there exists an  $\omega \in \mathbb{R}$ , called  $\epsilon$ -approximate eigenfrequency, such that

$$\| U^t z - e^{i\omega t} z \| \leq \epsilon \| z \| \quad (24)$$

where  $\epsilon$  can be made arbitrarily small as the embedding window  $Q$  increases. It is important to note that the symbol “ $\epsilon$ ” in this context is not the same as the kernel bandwidth parameter and is used to maintain consistency with the original concept presented in [Giannakis, 2021].

Hence, the approximation of irregular dynamics using Koopman eigenfunctions is prone to errors. In this study, we propose a modification to address this issue by assuming that some eigenfunctions  $\psi_i(x)$  may not evolve as completely single-frequency functions, as described in (2). This error can be compensated by coupling the eigenfunctions with each other. To achieve this, we use a linear evolution model with an  $l' \times l'$  matrix  $K_\psi$ :

$$\psi(x(t+1)) = K_\psi \psi(x(t)) \quad (25)$$

where  $\psi = (\psi_1, \dots, \psi_{l'})^T$  is a column vector including Koopman eigenfunctions and the matrix  $K_\psi$  is computed based on data as follows. First, we construct two matrices using Algorithm 1, which involve eigenfunction evaluations on sampled data:  $\Psi^- = [\psi(x_1), \dots, \psi(x_{N-1})]$  and  $\Psi^+ = [\psi(x_2), \dots, \psi(x_N)]$ . The matrix  $K_\psi$  is then determined as the solution of the following optimization problem:

$$\min_{K_\psi} \| \Psi^+ - K_\psi \Psi^- \|_2 \quad (26)$$

which is solved using normal equations .

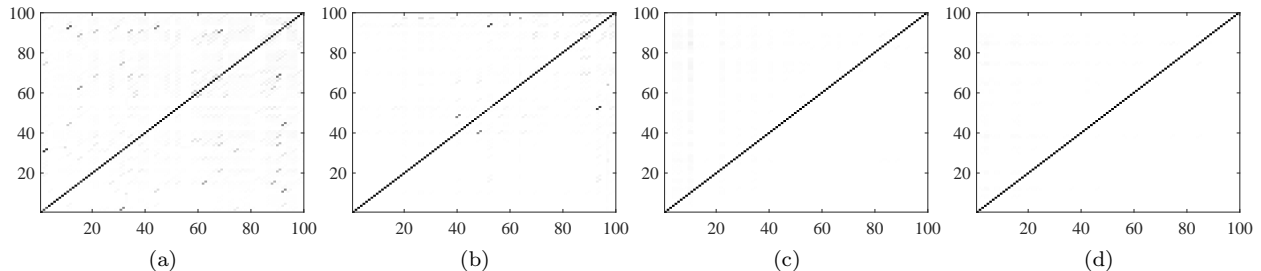


Figure 1: Visualization of  $K_\psi$  for different embedding windows indicates that, increasing  $Q$ , the utilized approach decomposes the dynamics into coherent patterns with each pattern having decoupled dynamics. (a)  $Q = 100$ , (b)  $Q = 500$ , (c)  $Q = 1000$ , (d)  $Q = 10000$ .

If the underlying dynamics is regular, such as periodic or quasiperiodic dynamics, the recovered eigenfunctions using the kernel operator and delay coordinate approaches are single-frequency. In this case,  $K_\psi$  will be block-diagonal since Koopman eigenfunctions are complex conjugate pairs that evolve in pairs, and each block will be a  $2 \times 2$  skew-symmetric matrix. However, for irregular dynamics, such as chaotic or mixing dynamics, some eigenfunctions may evolve through coupling with others, leading to a slightly broken block-diagonal structure. Figure 1 demonstrates this concept, showing that by increasing the embedding window,  $k_\psi$  gets closer to the ideal block-diagonal matrix. Specifically, for  $Q \geq 1000$ , our proposed approach recovers coherent patterns that align with exact Koopman eigenfunctions (with  $\epsilon$  values close to zero in (24)).

Another problem to consider before deploying the approach is the data-driven Koopman mode decomposition  $\hat{f}_j = \langle f, \psi_j \rangle$  required to evaluate (2). Due to the  $\epsilon$ -approximate eigenfunctions, the orthogonality of the recovered eigenfunctions, which is a necessary condition to derive (2), may not be satisfied with sufficient accuracy. Additionally, accurately evaluating the inner product  $\langle f, \psi_j \rangle$  requires a sufficient amount of data sampled over  $\mathcal{X}$ , and any data shortage will introduce errors. To reduce these types of errors, we propose using a linear decoder that maps Koopman eigenfunctions to system states with large enough set of Koopman eigenfunctions that spans the system state, i.e.  $x \in \text{span} \psi_k(x)_{k=1}^{l'}$ . Accordingly, the system state is expanded in terms of Koopman eigenfunctions through a  $d \times l'$  matrix  $C$  as follows:

$$x = C\psi(x) \quad (27)$$

where  $x \in \mathbb{R}^d$  represents the system state vector. To determine  $C$  based on available data, we formulate an optimization problem as follows:

$$\min_C \|X - C\Psi\|_2 \quad (28)$$

where  $X$  and  $\Psi$  are time-ordered matrices given by  $X = [x_1, \dots, x_N]$  and  $\Psi = [\psi(x_1), \dots, \psi(x_N)]$ .

## 5 Clustering the data

We employ a clustering-based Koopman approach to group power stations based on their temporal power patterns and then predict future energy production for each pattern. Generally, power generation follows a consistent pattern of evolution over time, which can be identified by mapping power temporal data to a lower dimensional space. Dimensionality-reduction methods such as PCA [Moon and Stirling, 2000], diffusion maps [Coifman and Lafon, 2006a], and t-SNE [van der Maaten and Hinton, 2008] are popular tools for the visualization of high-dimensional data. However, these methods have some limitations, such as sensitivity to noise, the scrambled global structure of data, computational scalability, and optimizing for two- or three-dimensional visualization. To address these concerns, a method based on the potential of heat diffusion for affinity-based transition embedding called PHATE was recently developed [Moon et al., 2019]. While the original work focused on biological data, in this study, we apply PHATE to detect distinct power generation patterns.

We first describe the process of normalizing a typical time-ordered vector  $x$  as

$$\hat{x} = \frac{x - x_{min}}{x_{max} - x_{min}} \quad (29)$$

where  $x$  has minimum and maximum values of  $x_{min}$  and  $x_{max}$  and  $\hat{x}$  denotes the normalized vector. For clustering, we consider the load data at  $d$  grid points as time-ordered vectors in  $\mathbb{R}^N$ . We denote the load recorded at station  $i$  as  $y_i = [y_i(t_1), \dots, y_i(t_N)]^T$ , where  $i = 1, \dots, d$  and measure the empirical similarities between different load patterns for the normalized vectors  $\hat{y}_i$  using a variable bandwidth kernel, as explained in Section 4.3. This leads to a kernel matrix, denoted as  $\hat{P}_{d \times d}$ , where the elements  $\hat{P}_{ij}$  indicate the similarity between each pair  $(\hat{y}_i, \hat{y}_j)$ . It is worth noting that evaluating similarities of spatial points does not involve any time-delay  $Q$ . Also the matrix  $\hat{P}$  used in PHATE to compute similarities between different time points differs from the matrix  $P$  used in Section 4.3—due to the difference between the vectors  $y_i \in \mathbb{R}^N$  and  $x_i \in \mathbb{R}^d$ .

After defining an initial diffusion operator like  $\hat{P}$ , PHATE proceeds with a few carefully designed steps. Firstly, the diffusion operator is raised to its  $t'$ -th power, where the optimal diffusion time scale  $t'$  is chosen based on von Neumann entropy. This provides a robust intrinsic data distance that preserves the global structure of the data and low-pass filters the data. To embed the global structure in low (two or three) dimensions and resolve instabilities, PHATE considers  $\hat{U}_i^{t'} = -\log(\hat{P}_i^{t'})$ , where  $\hat{P}_i^{t'}$  is the  $i$ -th row of  $\hat{P}^{t'}$ , and computes the potential distances:

$$\Gamma_{ij}^{t'} = \|\hat{U}_i^{t'} - \hat{U}_j^{t'}\|_2 \quad (30)$$

The final step involves performing a metric multidimensional scaling (metric MDS) to embed the data into a low-dimensional space (in our case, a 3-dimensional space). This is done by minimizing the following ‘stress’ function:

$$\text{stress}(\hat{z}_1, \dots, \hat{z}_d) = \sqrt{\frac{\sum_{i,j} (\Gamma_{ij}^{t'} - \|\hat{z}_i - \hat{z}_j\|)^2}{\sum_{i,j} (\Gamma_{ij}^{t'})^2}} \quad (31)$$

where the function operates on the embedded  $m$ -dimensional coordinates of data points. While the classical MDS assumes that input distances correspond to low-dimensional Euclidean distances, this assumption is overly restrictive for the PHATE setting. The metric MDS, however, relaxes this assumption by requiring only that the input distances be a distance metric. The entire clustering process is summarized in Algorithm 2.



---

**Algorithm 2** Low-dimensional embedding of data using PHATE for clustering

---

- Input
    - Time series of each station ordered as  $y_i = [y_i(t_1), \dots, y_i(t_N)]^T$ ,  $y_i \in \mathbb{R}^N$ ,  $i = 1, \dots, d$
    - Number of retained nearest neighbors  $k_{nn}$
  - Output
    - PHATE coordinates  $\text{PHATE}_j \in \mathbb{R}^d$
  - Steps
    - 1: Get the normalized data  $\hat{y}_i$  according to (29)
    - 2: Compute the  $d \times d$  pairwise distances  $d_1(\hat{y}_i, \hat{y}_j)$  using (10)
    - 3: For each  $i$  only retain the  $k_{nn}$  smallest values of  $d_1(\hat{y}_i, \hat{y}_j)$  and consider the set  $\mathcal{N}_{k_{nn}}(\hat{y}_i) = \{\hat{y}_j | \hat{y}_j \text{ in the } k_{nn} \text{ neighbourhood of } \hat{y}_i\}$
    - 4: Symmetrize  $d_1(\hat{y}_i, \hat{y}_j)$  by augmenting the list of retained distances for given  $i$  if  $\hat{y}_i \in \mathcal{N}_{k_{nn}}(\hat{y}_j)$  but  $\hat{y}_j \notin \mathcal{N}_{k_{nn}}(\hat{y}_i)$
    - 5: Determine the optimal bandwidth function  $\epsilon = \epsilon(\hat{y}_i, \hat{y}_j)$  using the procedure described in [Berry and Harlim, 2016]
    - 6: For  $d_1(\hat{y}_i, \hat{y}_j)$ , form the  $d \times d$  matrix  $\hat{K}$  in (10), treating all pairwise kernel values  $\hat{K}_{ij}$  not associated with the retained distance data as zero.
    - 7: For  $\hat{K}$ , compute the  $d \times d$  sparse matrix  $\hat{P}$  in (11)
    - 8: Compute an optimal value for the diffusion time scale  $t'$  using the algorithm given in [Moon et al., 2019]
    - 9: For each row  $\hat{P}_i^{t'}$  of  $\hat{P}^{t'}$  compute  $\hat{U}_i^{t'} = -\log(\hat{P}_i^{t'})$
    - 10: Compute the potential distances  $\Gamma_{ij}^{t'}$  in (30)
    - 11: Do a metric MDS by minimizing the ‘stress’ function (31) and obtain  $\hat{z}_i \in \mathbb{R}^m$ ,  $i = 1, \dots, d$ .
    - 12: Set  $\text{PHATE}_j = [\hat{z}_1(j), \dots, \hat{z}_d(j)]^T$ ,  $j = 1, \dots, m$ , where  $\hat{z}_i(j)$  denotes the  $j$ -th element of vector  $\hat{z}_i$ .
-

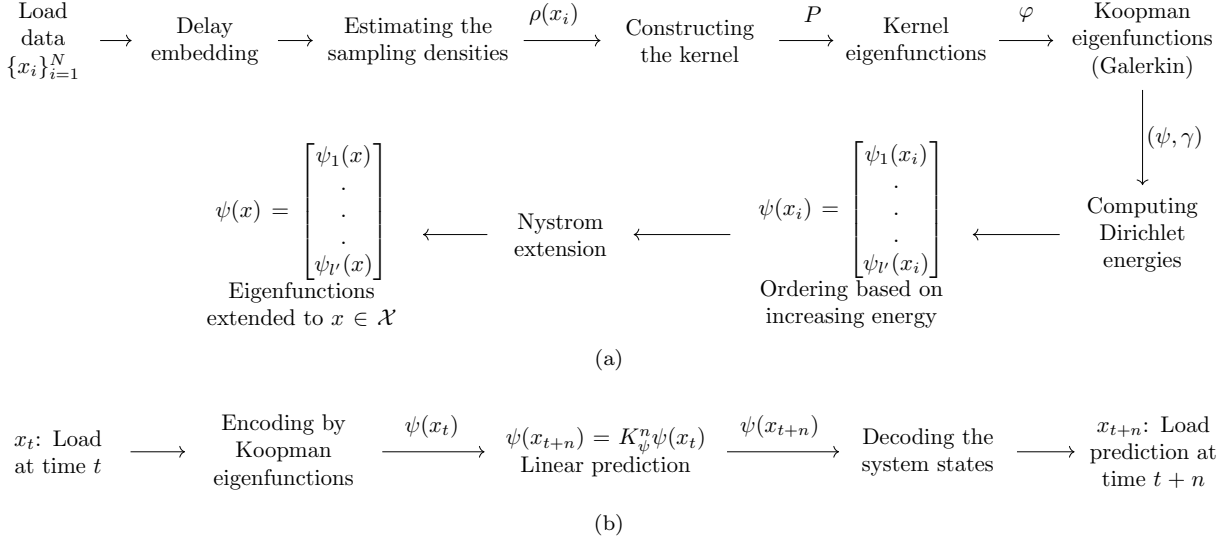


Figure 2: (a) Computing Koopman eigenfunctions. (b) Load forecasting using Koopman.

## 6 Results

Here, we present results from applying the Koopman operator approach to the data described in Section 6.1. Figure 2 illustrates a schematic of our proposed numerical approach for load forecasting using Koopman eigenfunctions. The performance of our approach is evaluated using the root mean squared error (RMSE).

$$\text{RMSE} = \sqrt{\frac{1}{n_x} \sum_{i=1}^{n_x} (x_i - x_i^f)^2} \quad (32)$$

which applies to a vector  $x = [x_1 \dots x_{n_x}]^T$  and its forecasted value  $x^f = [x_1^f \dots x_{n_x}^f]^T$ . Throughout this paper, all error and RMSE values were computed using normalized load vectors, limiting the RMSE to the range of 0 to 1.

### 6.1 Data description

This paper utilizes a dedicated and large-scale data set for a renewable electric power system [Jensen and Pinson, 2017] from the continental European electricity system collected for the period of 2012-2014 and includes data on demand and renewable energy inflows with a high resolution of 50 km and 1 hour. The dataset covers mainland Europe and 3 years and consists of a transmission network model, as well as information for generation and demand. The data was collected from 1494 transmission buses with 2156 lines, including conventional generators with their technical and economic characteristics, as well as weather-driven forecasts and corresponding realizations for renewable energy generation. Figure 3 provides an overview of the dataset and the power grid.

### 6.2 Reduced-order modeling of the load dynamics

Many high-dimensional systems of interest often evolve on low-dimensional manifolds or attractors, which can be well-approximated using a low-rank basis [Brunton et al., 2016]. We show that the Koopman eigenfunctions yield a natural such basis for the load dynamics. By applying Algorithm 1 to load data from January 2014 with a delay of  $Q = 500$  and a regularizing parameter of  $\theta = 10^{-9}$ , we identified 100 Koopman eigenfunctions and used them to reconstruct the load for all 1494 stations during that month. Example load reconstructions are shown in Figure 4. This same approach can be used to reconstruct the load for other months or over larger time horizons, though doing so may require increasing the length of the delay, which presents computational challenges due to the large amounts of data involved.

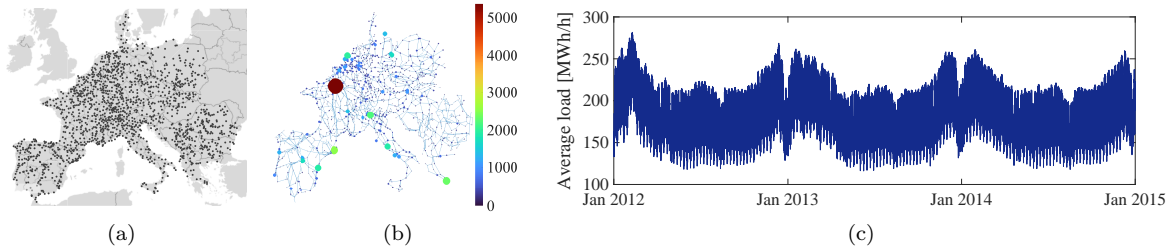


Figure 3: Overview of dataset. (a) Distribution of generators. (b) Transmission grid and the 3-year average power of each generator in MWh/h. (c) Average load of all power plants. The sampling rate is 1 hour and the load .

### 6.3 Nonlinear spatiotemporal spectral analysis of the load dynamics

The Koopman eigenfunctions effectively capture spatiotemporal load dynamics, encoding them on a low-order manifold. This yields coherent patterns in the NLSA space [Giannakis and Majda, 2012, 2013], and highlight the most predictable and robust features of the evolving dynamics [Giannakis et al., 2018; Froyland et al., 2021; Giannakis, 2021]. By applying Algorithm 1 to the data of each month, we obtain the coherent patterns associated with that month. For example, Figure 5 depicts these patterns, with the least Dirichlet energy values in Koopman eigenfunctions, for January 2014. While temporal modes of different months are similar, the spatial modes associated with different months might be generally different (see Figure 6).

Figure 5 reveals that the dominant frequencies contributing to load dynamics scale with zero, one month, one week, one day, and half a day. These load dynamic components have physical interpretations, for example the zero-frequency mode corresponds to the average loads generated in individual power stations (compare the spatial pattern in the first row of Figure 5 to average loads in Figure 3). The mode scaling with one month in the second row of Figure 5 is due to monthly weather changes, e.g. temperature and solar radiation. Additionally, the modes in the third row of Figure 5, representing a weekly frequency, are influenced by working days and holidays, while the mode scaling in the fourth row of Figure 5, corresponding to a daily frequency, is affected by changes in solar radiation over 24 hours. The final row in Figure 5 displays a half-day frequency, which indicates variations in power usage patterns during day and night.

The Koopman operator enables the identification of multiscale dynamics and the detection of mode contributions at various scales in power grids. Unlike conventional Fourier analysis and POD methods [Holmes et al., 1996] which decompose signals into their frequency components, the Koopman operator spectra optimally decompose dynamics into nonlinear basis functions [Lange et al., 2021], specifically Laplace-Beltrami operator eigenfunctions [Giannakis and Majda, 2012] that characterize the geometry of the nonlinear data manifold [Coifman and Lafon, 2006a]. Unlike conventional methods which primarily extract temporal patterns, the optimal basis discovered from Koopman spectral analysis determines spatial patterns corresponding to each temporal mode, as seen in the right column of Figure 5. Moreover, no prior knowledge of a base frequency is necessary for Koopman modal analysis.

The middle column of Figure 5 illustrates that the nonlinear load signal can be accurately reconstructed through a small number of highly predictable modes that exhibit near-periodic behavior. In contrast, the left column of Figure 5 shows that each mode has a narrow frequency band, reflecting intermittent patterns that play a crucial role in capturing features of strongly nonlinear dynamics [Giannakis and Majda, 2012, 2013].

### 6.4 Power usage patterns detected by spatial modes

The right column in Figure 5 shows that each Koopman eigenfunction elicits a distinct spatial pattern for its corresponding mode. While the spatial modes linked to zero and low frequencies in the upper three rows of Figure 5 are marked by the station that generates the largest average value in Figure 3, which is a station in France, the two last rows of Figure 5 highlight that high-frequency modes, scaled with a day and a half day, produce dissimilar patterns. In particular, the mode scaled with a day shows two stations in Northern Europe (Germany), and additional stations in Southern Europe (Italy, Greece, and Spain), which exhibit

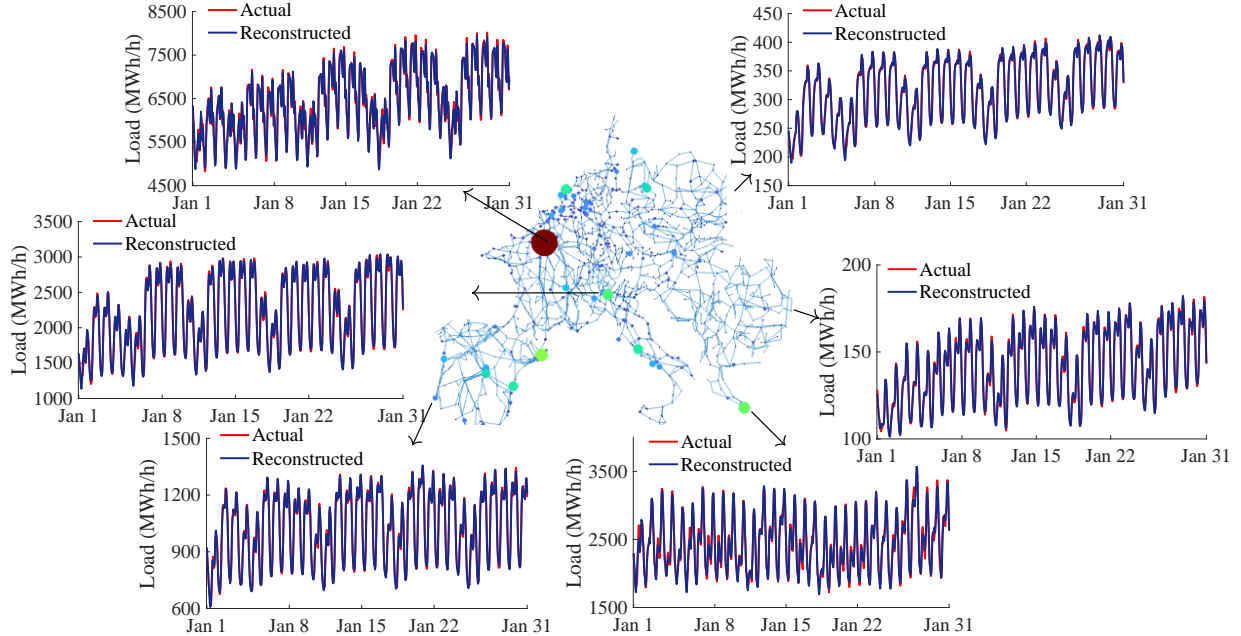


Figure 4: Examples of spatiotemporal load reconstruction. The load data of 1494 stations during January 2014 are reconstructed using 100 Koopman eigenfunctions.

the most significant amplitude in this mode. Moreover, as observed from the last row of Figure 5, these southern stations, after the one in France, generate the highest values in the mode scaled with a half day. This indicates different stations generating power for different purposes, with stations that produce power for industrial usage representing the largest values in low-frequency modes, while stations supplying power for residential and commercial areas manifest the higher-frequency (day and half day) modes.

Examining different spatial modes across various months elucidates the seasonal alterations in energy patterns. Figure 6 displays the spatial patterns corresponding to frequency scaled over a 24-hour period throughout the twelve months of 2014; for example in Figure 6, certain stations in Southern Europe exhibit distinctive modes during the winter months, yet their contribution diminishes during the warmer months spanning June 2014 to October 2014. Consequently, power usage in these regions remains relatively constant throughout the day in the warmer months but varies significantly during the colder months.

## 6.5 Clustering the data

Our rationale for utilizing cluster-based analysis is rooted in the ability to decompose the Koopman operator according to the sparse structure of the underlying dynamical system. This approach considers the system as a collection of interconnected subsystems, whose eigenfunctions induce corresponding eigenfunctions for the entire system [Schlosser and Korda, 2022]. While the original research in [Schlosser and Korda, 2022] necessitates prior knowledge of the dynamics model for detecting sparsity and decomposing the system, we present an unsupervised method that employs PHATE [Moon et al., 2019] to detect sparsity and associated subsystems from data. Additionally, our approach deviates from the original variant in [Moon et al., 2019] by employing variable bandwidth kernels [Berry and Harlim, 2016] in the PHATE algorithm.

Applying Algorithm 2 to normalized data from 2012-2014 yields the upper plot in Figure 7, where we identify 10 clusters via  $k$ -means algorithm [Bishop, 2006]. The lower plot in Figure 7 demonstrates a clustering pattern that correlates with the physical graph of power plants, with stations in different geographical areas falling into different clusters. Figure 7 also reports clusters with completely synchronized stations, i.e., the clusters 2, 3, 4, 6, and 7, which correspond to groups that depart and unify distinctly from the main body in the upper plot of Figure 7. Additionally, clusters 1 and 10 are separated from the main body in the upper Figure 7, allowing for further extraction of groups of synchronized stations by either increasing

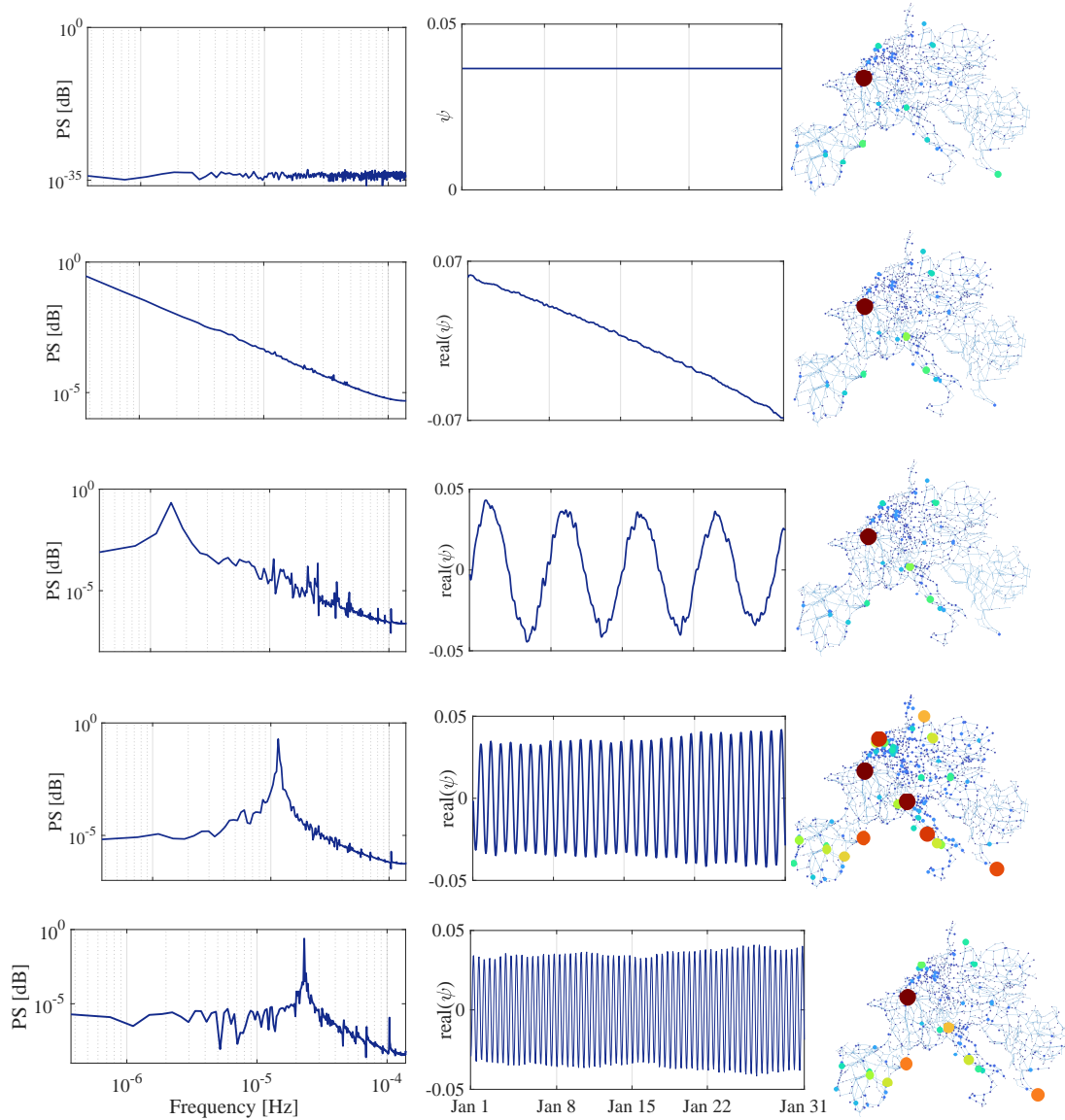


Figure 5: Spatial and temporal patterns with multiple scales recovered by the load data during January 2014. The left, middle, and right columns display the Power Spectrum (PS), time evolution, and spatial pattern induced by the Koopman eigenfunction, respectively. The first row represents the trivial Koopman eigenfunction ( $\omega = 0$ ), followed by subsequent rows associated with frequencies scaled with a month ( $3.86 \times 10^{-7}$ Hz), a week ( $1.65 \times 10^{-6}$ Hz), a day ( $1.15 \times 10^{-5}$ Hz), and a half day ( $2.31 \times 10^{-5}$ Hz), arranged in ascending order.

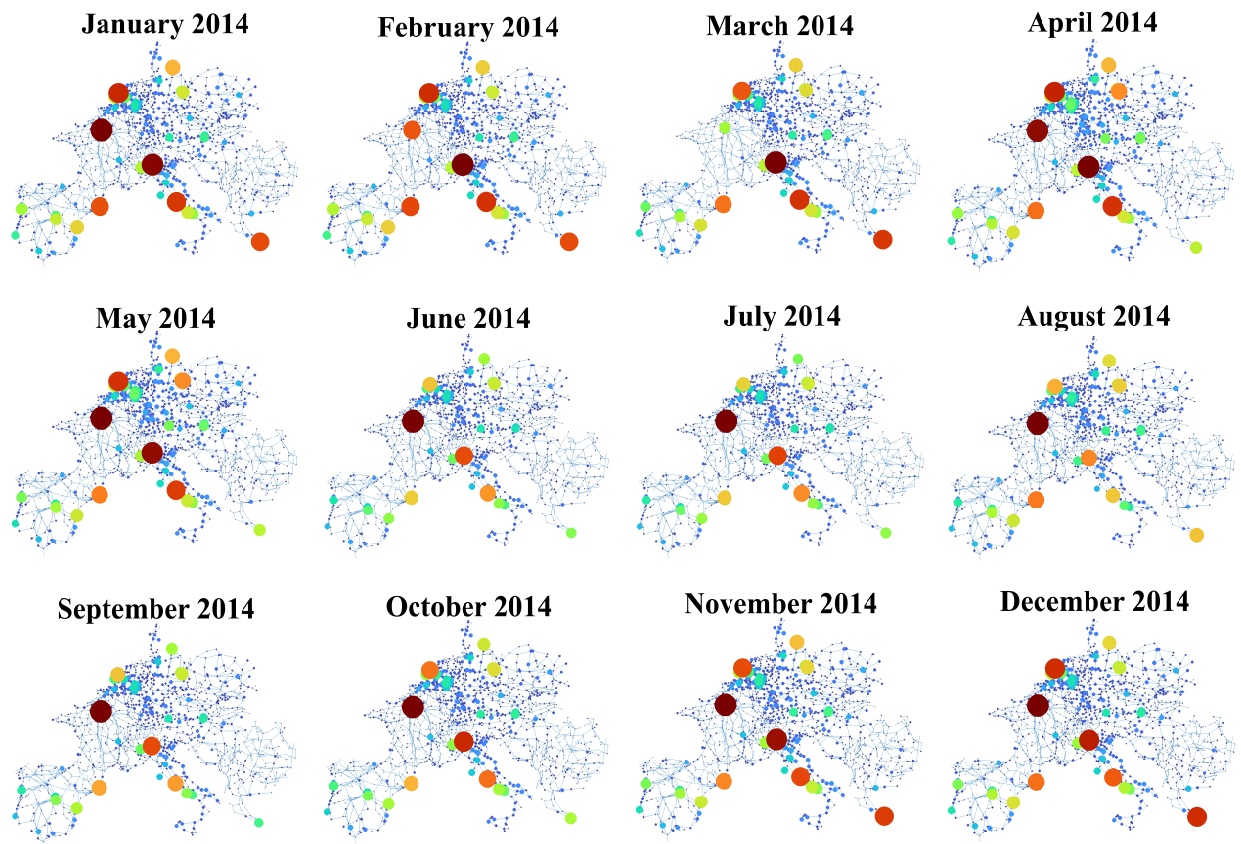


Figure 6: Extracted spatial patterns showing the frequency scaled with a day.

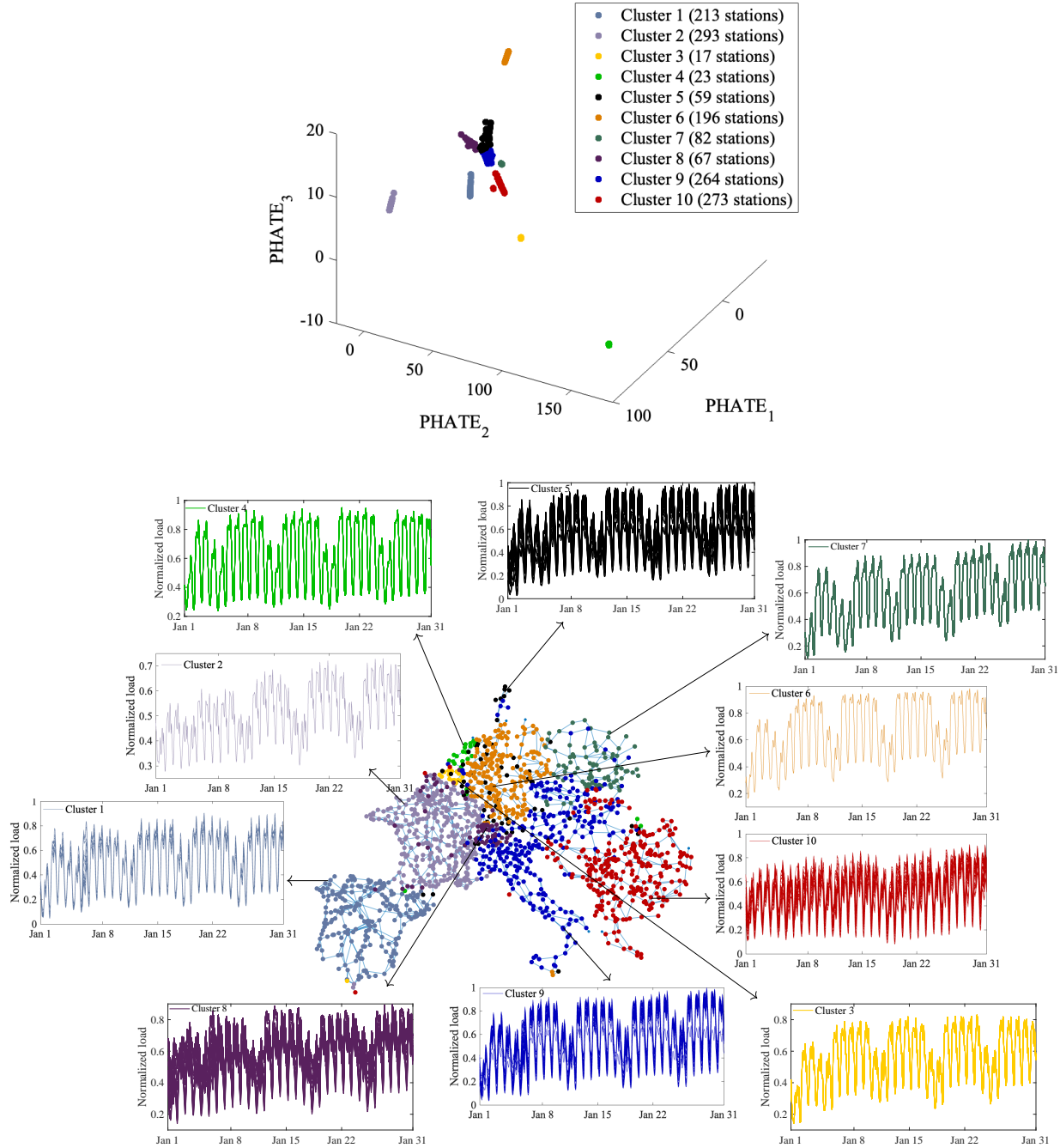


Figure 7: Visualizing the data on the low-dimensional PHATE coordinates unveils 10 clusters.

the number of clusters in the  $k$ -means approach or re-clustering the current clusters. Despite the potential for increased accuracy with more clusters, we opt for 10 clusters and make a trade-off between accuracy and model complexity. Overall, this clustering approach enables the identification of different power generation patterns and the division of the large-scale system into several interconnected subsystems.

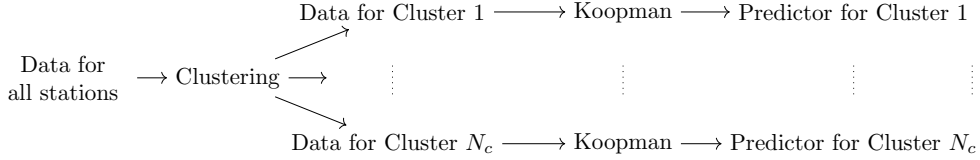


Figure 8: Cluster-based prediction of load.

## 6.6 Short-term load forecasting

Short-term load forecasting serves as a crucial factor in daily and weekly dispatching of power grids (Kong, 2020). To forecast a week ahead, we utilize Koopman modes from the previous week based on load data. This assumes no significant changes in Koopman modes occur between two successive weeks. Any significant changes to these modes, such as weather or holidays, may introduce errors. Nonetheless, our proposed approach outperforms a deep learning-based load forecasting method.

To facilitate forecasting, we employ a hierarchical approach (depicted in Figure 8) utilizing Algorithm 2 to cluster power stations. Load predictions are then generated for individual stations within each cluster through the construction of a single Koopman model for that cluster. As detailed in Section 6.5, we construct 10 Koopman models based on our analysis of load data.

The numerical evaluation of the Koopman operator necessitates tuning several parameters, among which the number of delays  $Q$  and Koopman eigenfunctions  $l'$  hold significant influence. Increasing the number of delays improves the extraction of highly coherent dynamical behaviors, as evidenced by Figure 1, which shows more regular and decoupled eigenfunctions—in the limit of infinitely many delays one can recover the exact dynamical system properties [Das and Giannakis, 2019; Giannakis, 2021]. However, practical limitations in data availability restrict the number of delays that can be used. Moreover, for the finite-dimensional Koopman subspaces, the delay embedding window shows some correlation with the frequency ranges of interest [Giannakis et al., 2018; Marrouch et al., 2020; Giannakis, 2021; Froyland et al., 2021], so that including uncorrelated delays may ignore the dynamical features in these ranges.

To investigate the role of delay horizon  $Q$  in load forecasting, we fix the number of eigenfunctions and compute the RMSE for each station. Figure 9 shows the results for 12 months of 2014, with  $l = 100$ . The RMSE values exhibit a minimum at  $Q = 200$  for the majority of the months, as demonstrated in Figure 9. Moreover, the RMSE values remain relatively stable as  $Q$  increases above 200, highlighting the robustness of the proposed technique with respect to the pivotal parameter  $Q$ . Given a sampling rate of one hour, 168 samples are available per week, thereby indicating that a delay time proportional to the forecasting horizon (one week in this instance) is reasonable for short-term forecasting. Notably, in cases where there are abnormal weather conditions or substantially noisy data, it may be possible to enhance the accuracy by increasing the delay horizon (e.g., November in Figure 9). Nonetheless, we must be mindful of the data’s accessibility and increased complexity in terms of computation and modeling. Hence, we advocate for a delay scaled to the forecasting horizon, but maintain caution when dealing with abnormally noisy data or weather conditions. In such instances, the proposed technique allows for the flexibility to increase the delay horizon to obtain more robust Koopman modes.

The number of Koopman eigenfunctions included in the forecasting model is the next parameter we investigate. While a rich library of eigenfunctions theoretically captures dynamical features across a wide spectrum, this does not necessarily translate to arbitrarily large libraries for real-world data. Including Koopman eigenfunctions with higher energy levels is often associated with computational errors and instability, potentially leading to false information. In practice, these higher modes may not be accurately approximated from finite datasets, as they are not well-behaved on the data manifold [Giannakis, 2019]. Additionally, the use of modes with little variance and no physical significance may not improve model interpretability. Overfitting in the regression problem (28) is also a concern when the library  $\Psi$  is excessively large [Giannakis, 2019; Tavasoli et al., 2023].

Figure 10 presents the RMSE values for varying values of  $l'$  with a delay horizon of  $Q = 168$ . In the majority of months depicted in Figure 10, the RMSE attains a minimum (in terms of the RMSE distribution of individual stations and/or the mean value) at intermediate  $l'$  values (approximately  $l' = 50$ ). This



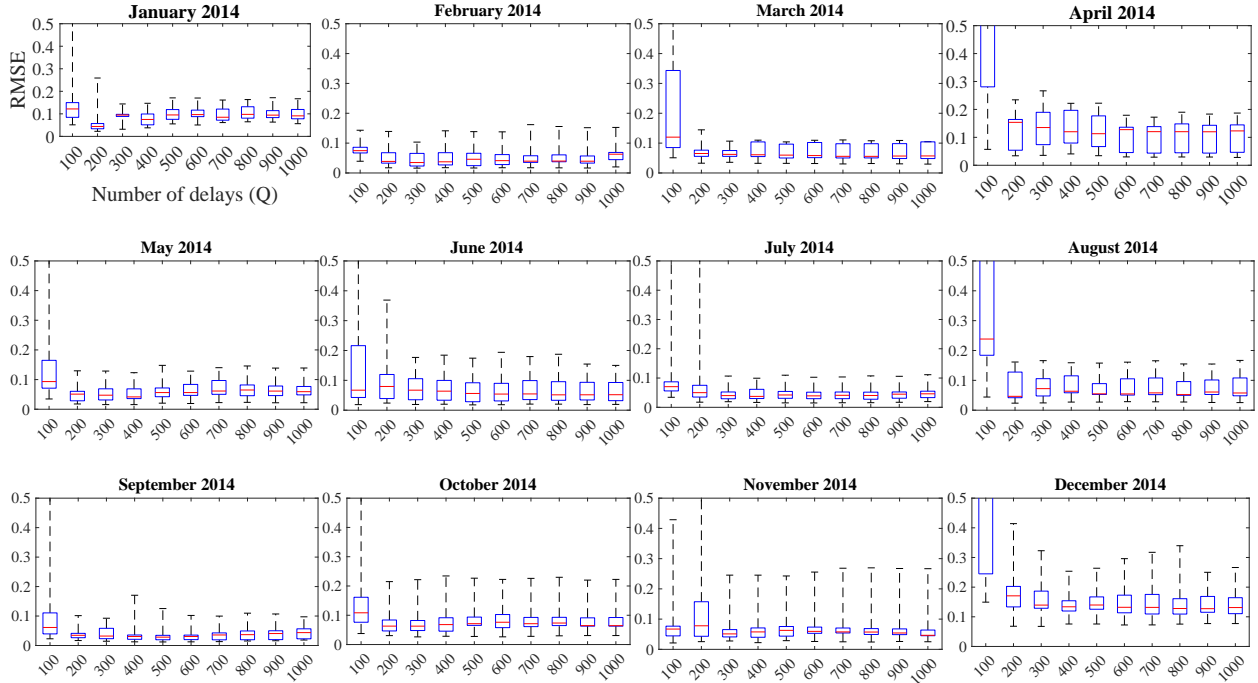


Figure 9: RMSE of different stations at varying values of time delay in different months ( $l' = 100$ ).

observation suggests that a library that is too extensive can result in overfitting when  $l'$  is increased beyond the intermediate range.

Figure 11 shows the RMSE values for different stations and different months of 2014, when  $Q = 168$  and  $l' = 50$ . We apply these parameters to various Koopman models for different clusters and months. The results demonstrate that the lowest forecasting errors occur during the winter and summer months, while errors are generally larger during spring and fall. In addition, Figure 11 reveals the largest errors in June, November, and December. Therefore, irrelevant features that may originate from noisy data or exogenous effects, such as weather conditions or public holidays, could contribute to forecasting errors. Specifically, the exceptionally high errors observed in April 2014 are attributed to public holidays.

To elucidate further, we present a load example for the final two weeks of April 2014 in Figure 12, aimed at providing a more detailed examination of this particular month. We also show the RMSE for April 2014 for the extended delay window  $Q = 500$  (see the right side of Figure 12). Analysis of the load pattern on the left side of Figure 12 highlights the occurrence of two public holidays on April 18 (Friday) and April 22 (Monday), resulting in a notable reduction in correlation between the training and test datasets, namely between the final two weeks of April 2014. Moreover, comparing the right side of Figure 12 with the corresponding RMSE for April 2014 in Figure 11, we observe more accurate forecasting and a considerable decrease in errors upon increasing the delay to  $Q = 500$ . Thus, we confirm the crucial role of delay embedding in comprehending the intricate load dynamics and achieving robust forecasting in the presence of exogenous factors.

Figure 13 further demonstrates the performance of the proposed approach by showcasing examples of load forecasting in January 2014. We use the same parameters, i.e.,  $Q = 168$ ,  $l' = 50$ , and  $\theta = 10^{-9}$ , for different Koopman models regarding different clusters and different months in Figures 11 and 13.

## 6.7 Comparison with deep learning

In this paper, we employ an approach that involves unfolding and decomposing the data manifold structure to investigate the system dynamics. By doing so, we avoid the limitations of a conventional search that considers an opaque and amorphous environment, and instead utilize the loaded data in a targeted manner. As previously demonstrated, this approach provides a clear representation of the dynamics and ample room

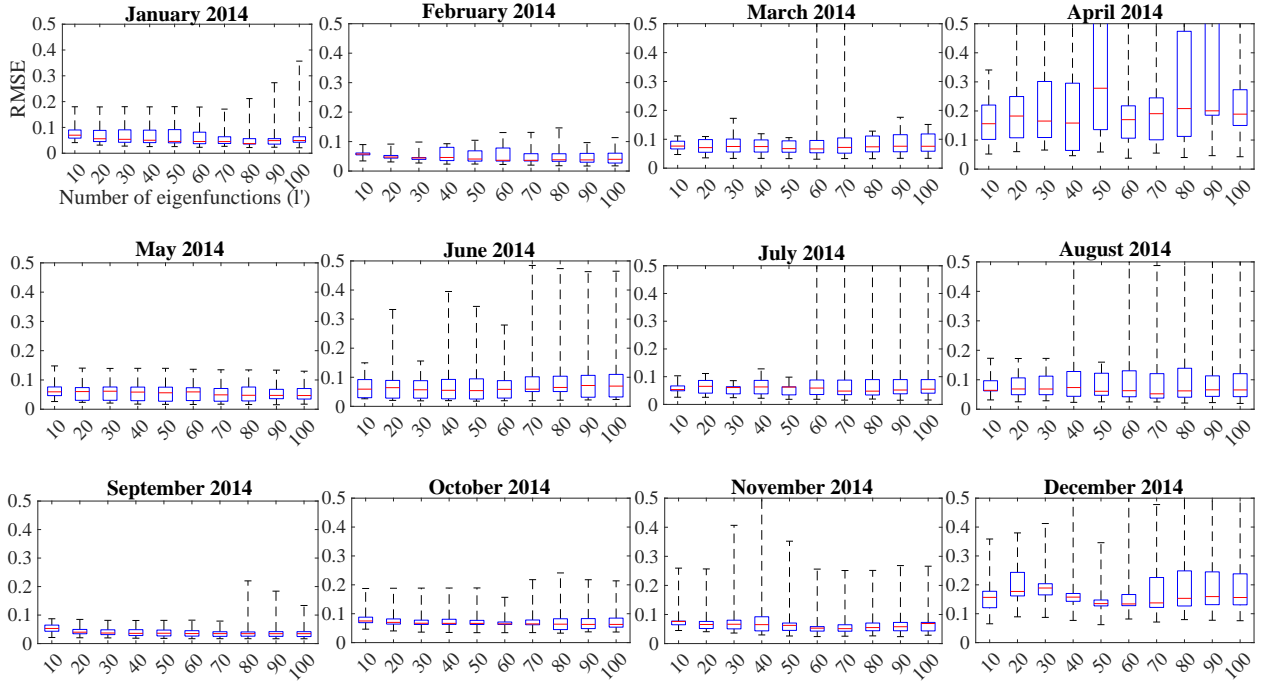


Figure 10: RMSE of different stations at varying values of number of Koopman eigenfunctions in different months ( $Q = 168hr$  (one-week delay)).

for analysis and interpretation. Here, we highlight its superiority over the LSTM method, commonly used in load forecasting, as evidenced by prior research [Marino et al., 2016; Kong et al., 2019; Peng et al., 2021; Zhu et al., 2022]. Our proposed method offers higher accuracy and computational feasibility.

Figure 14 compares the RMSE values for different clusters and different months of 2014. For Koopman, we used  $l' = 50$  eigenfunctions with a delay of  $Q = 168$ . The LSTM utilized a two-layer architecture with 100 hidden units in each layer, and tanh activation function. The Adam optimizer is used for gradient descent with mean squared error (MSE) loss function, and the batch size of 64 with 10000 epochs. To prevent over-fitting, we used a dropout unit with a rate of 0.2 after each LSTM layer. Both methods predicted short-term forecasts for the final week of each month, with one week of training data. The LSTM parameter values were tuned to minimize forecasting errors while avoiding overfitting. Increasing the number of LSTM layers, hidden units, or epochs beyond the specified values resulted in overfitting. Accordingly, we designed a PHATE cluster-based LSTM to conduct a cluster-based forecast, as depicted in Figure ???. Compared to our approach, the LSTM is not interpretable and it is significantly more complex, employing a two-layer architecture with 100 hidden units in each layer, while the Koopman approach utilizes a mere 50 modes. Consequently, on equivalent computing machinery, the LSTM requires  $\times 36$  more time for forecasting a month.

Overall, Figure 14 exhibits lower forecasting error in the Koopman approach. However, an exception is observed in April; as discussed in Section 6.6, certain exogenous factors (e.g. public holidays) in the second last week of April 2014 resulted in less coherent modes for delay horizon  $Q = 168$ . To address this, increasing the delay to  $Q = 500$  (as shown in Figure 15 on the left) yielded comparable forecasting results to LSTM. Figure 15 also demonstrates that widening the embedding window led to improved forecasting for clusters 3 and 7 in November and December (compare clusters 3 and 7 in the middle and right panels of Figure 15 with their respective plots in Figure 14).

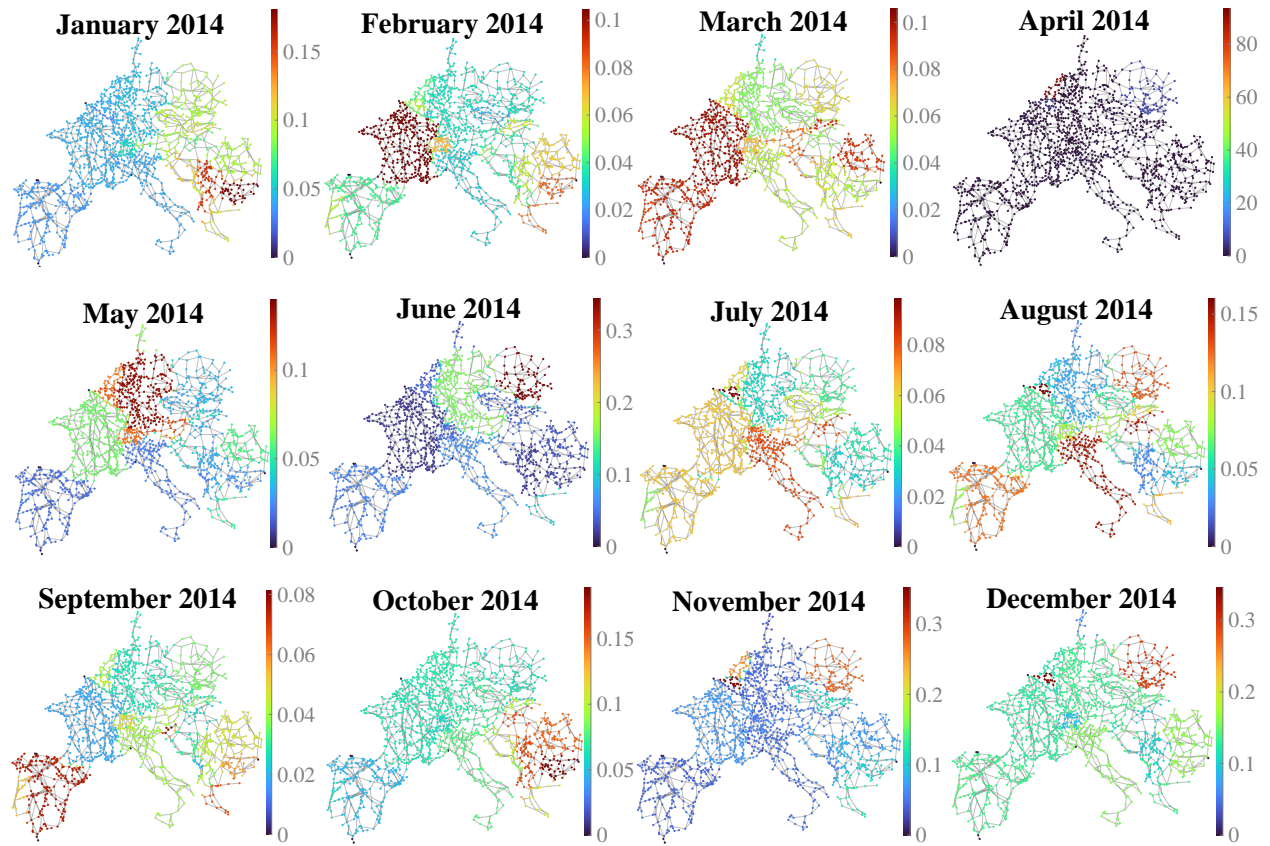


Figure 11: RMSE for different months with  $Q = 168hr$  (one-week delay) and  $l' = 50$ .

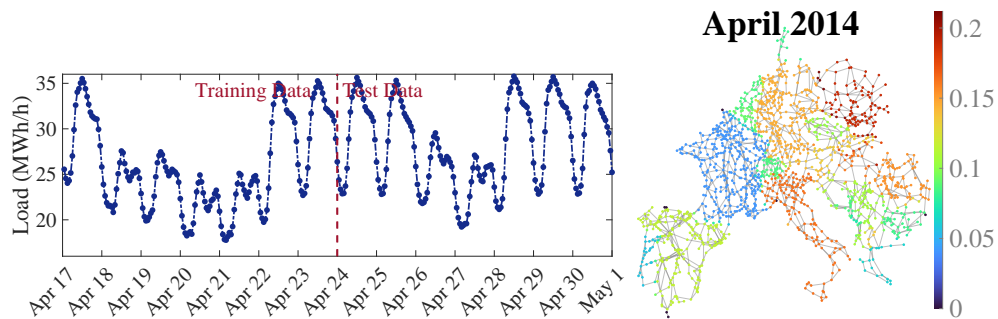


Figure 12: A load example (left) and the RMSE (right) for April 2014 with  $Q = 500$  ( $l' = 50$ ).

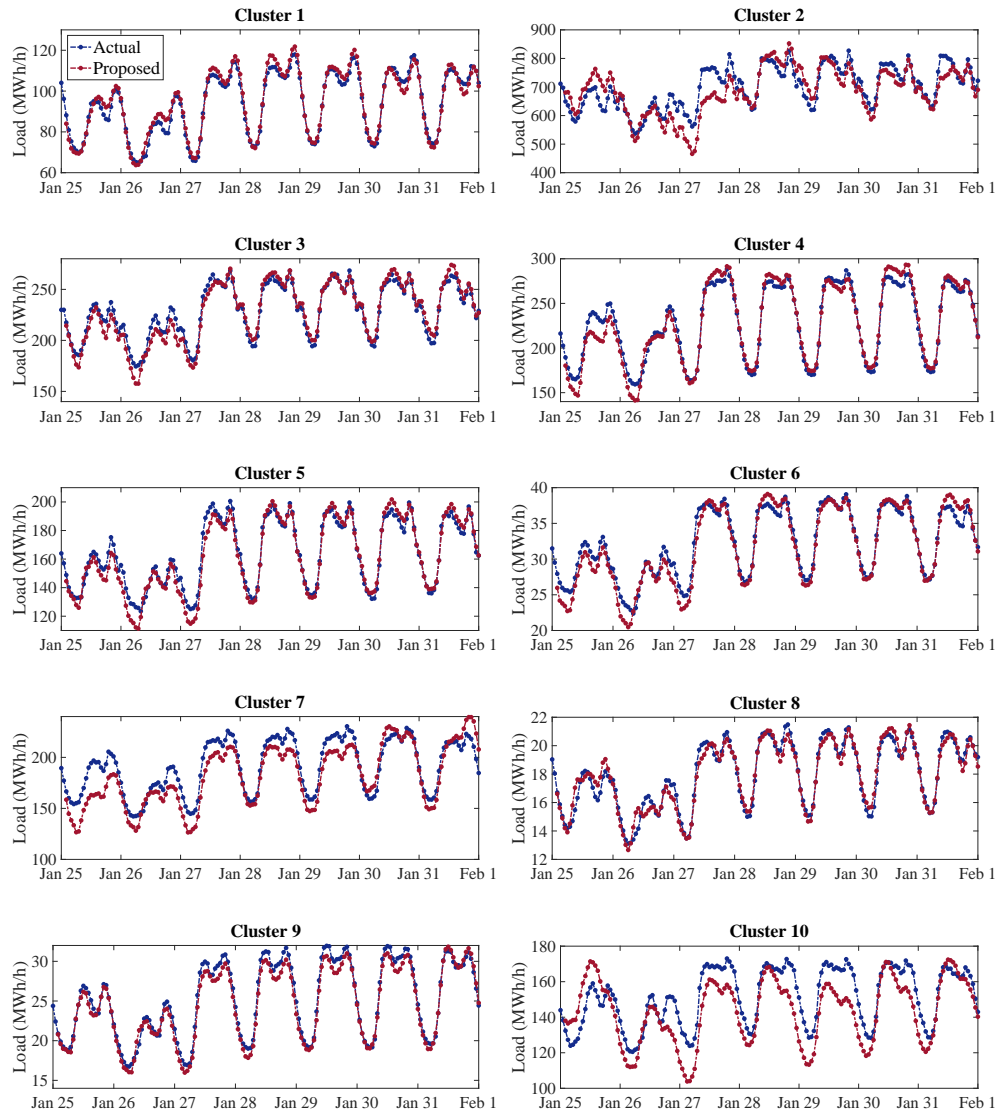


Figure 13: Examples of forecasted load in last week of January 2014 ( $Q = 168hr$  (one-week delay),  $l' = 50$ ).

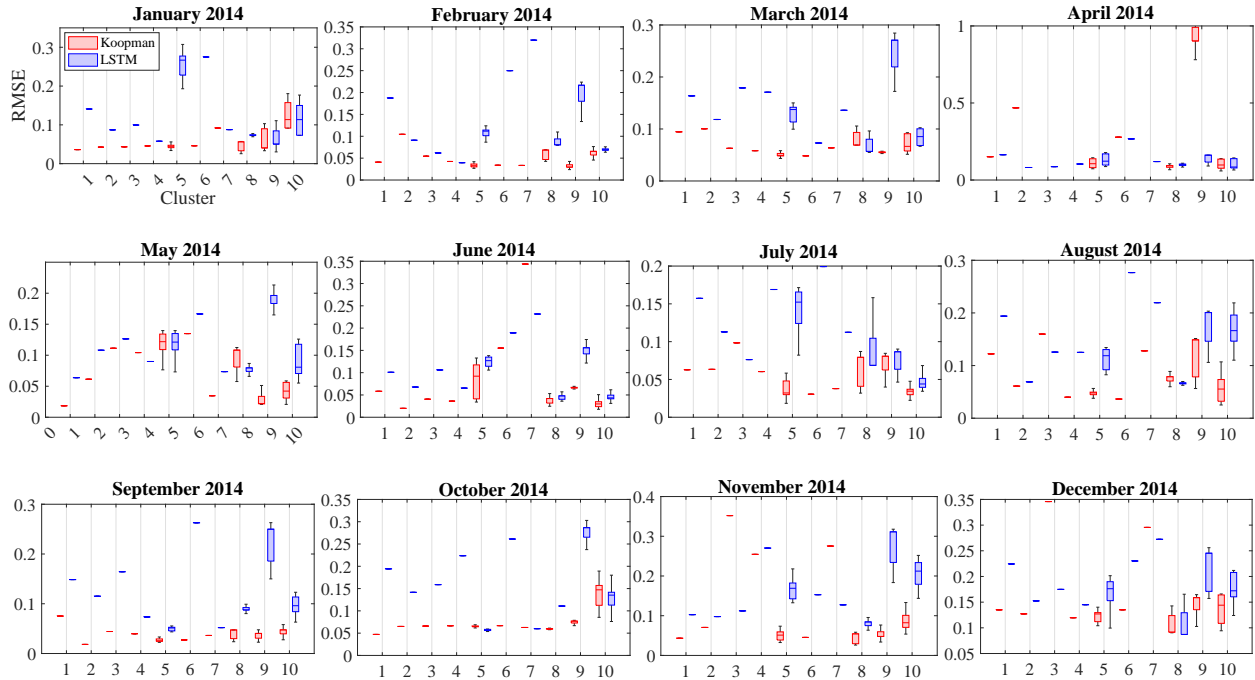


Figure 14: RMSE values due to Koopman and LSTM for different clusters in the last week of each month in 2014.

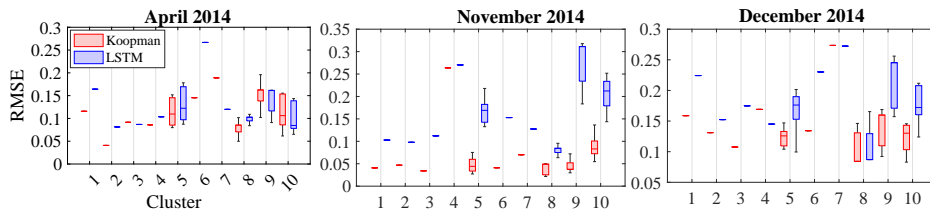


Figure 15: Comparing LSTM and the Koopman with  $Q = 500$ .

## 6.8 Modal noise and innovation noise

By expressing the load dynamics using Koopman eigenfunctions (refer to Equation (27)), it is possible to differentiate between various sources of forecasting errors and detect modal and innovation noises [Mohr et al., 2022]. In particular, due to the truncation of the infinite-dimensional Koopman operator, the finite-dimensional expansion  $C\psi(x)$  introduces a residual  $r$  in relation to the actual load data  $x$ , such that  $x(t) = C\psi(t) + r(t)$ . Hence, we split the residual  $r$  into modal noise  $\eta_m$  and innovation noise  $\eta_i$  as follows:

$$\begin{aligned}\eta_m(t) &= CC^\dagger r(t) \\ \eta_i(t) &= (I - CC^\dagger)r(t)\end{aligned}\tag{33}$$

where  $I$  is the identity matrix and  $C^\dagger$  is the Moore-Penrose pseudo-inverse of  $C$ . Therefore,  $\eta_m$  is in the plane of truncated Koopman eigenfunctions, while  $\eta_i$  remains perpendicular to this plane. Adding more eigenfunctions extends the modal plane and reduces innovation noise. However, modal noise is caused by mismatch in the regression matrix  $C$  between training and test data and cannot be reduced by adding more Koopman eigenfunctions. Therefore, the optimal number of Koopman eigenfunctions can be determined based on this criterion [Mohr et al., 2022].

We analyze modal and innovation noise in power grids for January 2014, considering cases with and without measurement noise. In each case, we compute the residuals for all 168 hours of the last week of January 2014 and for all stations. Figure 16 shows the case without measurement noise (original data without adding noise). The upper row exhibits significant modal noise, while the lower row's innovation noise decreases with more Koopman eigenfunctions. This suggests that a few Koopman eigenfunctions suffice to capture effective dynamics modes in power grids, and the residual remains in this space. Improving forecasting involves modifying matrix  $C$  and accurately evaluating Koopman mode contributions in load dynamics evolution. This could involve incorporating exogenous effects, such as weather and public holidays, to modify the contribution of Koopman eigenfunctions in the training data for the test data's load dynamics evolution.

Next, Figure 17 shows the case with measurement noise, where we have manually added 10% noise into the original data. Here, the innovation noise changes slightly by increasing the number of Koopman eigenfunctions in the lower row of Figure 17. The Koopman approach enables us to differentiate the error caused by regression mismatch (upper row) from that due to measurement noise (lower row). Since the added noise lacks dynamics, it does not fall within the Koopman eigenfunctions' span. Thus, the Koopman model distinguishes between low-energy dynamic components and high-energy noisy parts, making no attempt to capture noise dynamics.

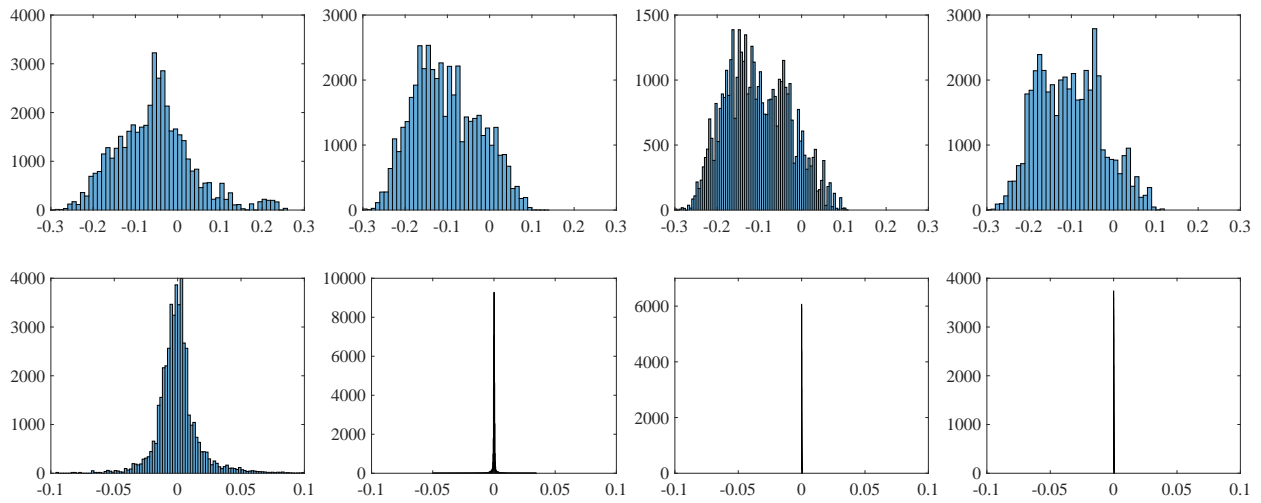


Figure 16: Original data (without added noise): Modal (upper row) and innovation (lower row) noise for load forecasting of all stations during 168 hours of last week of January 2014. Ordered from left, the columns show the results for  $l' = 5, 10, 20, 50$  Koopman eigenfunctions.

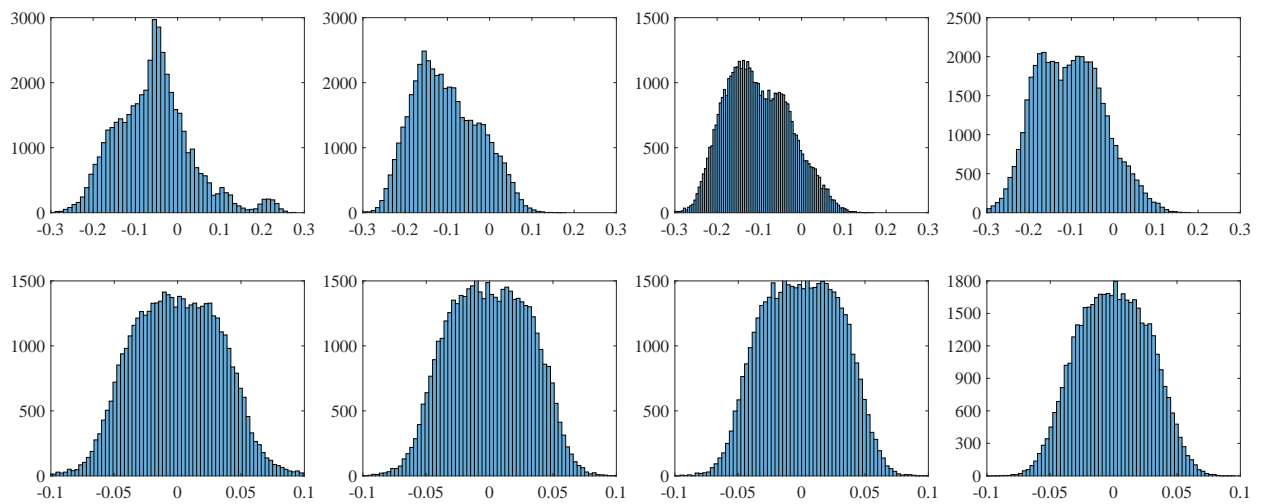


Figure 17: 10% noise included: Modal (upper row) and innovation (lower row) noise for load forecasting of all stations during 168 hours of last week of January 2014. Ordered from left, the columns show the results for  $l' = 5, 10, 20, 50$  Koopman eigenfunctions.

## 7 Conclusion

In this paper, we propose a data-driven method to identify the load dynamics of power grids using the Koopman operator approach. Our method identifies a reduced-order model for load dynamics by extracting coherent spatiotemporal patterns based on a Koopman mode decomposition. These patterns provide a linear representation of the dynamics, allowing for spatiotemporal spectral analysis and the discovery of basic energy patterns in multiple time scales. We implement a cluster-based Koopman approach for load forecasting over large-scale power grids, using a clustering approach based on PHATE to detect synchronized load profiles and construct a single forecasting model for them. Our approach is compared to a deep learning approach and found to be more computationally efficient and better suited for large-scale power grids. Our method creates a bridge between physics-based and data-driven approaches, allowing for the discovery of hidden dynamical features of interconnected subsystems and exogenous effects in a nonparametric setting.

A natural extension of this approach will be improving the extracted coherent patterns, since they are crucial for forecasting and analysis. The first direction will be realizing the patterns in the presence of varying dynamical features, where Koopman modes may change weekly, due to abnormal (out of dynamics) weather conditions, holidays, or other changes in interconnected dynamics and exogenous effects. This may be done by a time-varying realization of Koopman eigenfunctions and by extending the existing online DMD approaches [Zhang et al., 2019; Alfatlawi and Srivastava, 2020]. The second direction is distilling the set of extracted coherent patterns by detecting and cleaning the spectral pollution, which is the appearance of spurious eigenvalues due to numerical errors of discretization that are unrelated to the underlying dynamics [Colbrook et al., 2023].

## References

- G. Filatrella, A. H. Nielsen, and N. F. Pedersen, “Analysis of a power grid using a kuramoto-like model,” *The European Physical Journal B*, vol. 61, no. 4, pp. 485–491, 2008. [Online]. Available: <https://doi.org/10.1140/epjb/e2008-00098-8>
- A. E. Motter, S. A. Myers, M. Anghel, and T. Nishikawa, “Spontaneous synchrony in power-grid networks,” *Nature Physics*, vol. 9, no. 3, pp. 191–197, 2013. [Online]. Available: <https://doi.org/10.1038/nphys2535>
- P. H. J. Nardelli, N. Rubido, C. Wang, M. S. Baptista, C. Pomalaza-Raez, P. Cardieri, and M. Latva-aho, “Models for the modern power grid,” *The European Physical Journal Special Topics*, vol. 223, no. 12, pp. 2423–2437, 2014. [Online]. Available: <https://doi.org/10.1140/epjst/e2014-02219-6>
- A. T. Saric, A. A. Saric, M. K. Transtrum, and A. M. Stankovic, “Symbolic regression for data-driven dynamic model refinement in power systems,” *IEEE Transactions on Power Systems*, vol. 36, no. 3, pp. 2390–2402, 2021.
- K. Wang, J. Wang, B. Zeng, and H. Lu, “An integrated power load point-interval forecasting system based on information entropy and multi-objective optimization,” *Applied Energy*, vol. 314, p. 118938, 2022. [Online]. Available: <https://www.sciencedirect.com/science/article/pii/S0306261922003579>
- Y. Hu, X. Cheng, S. Wang, J. Chen, T. Zhao, and E. Dai, “Times series forecasting for urban building energy consumption based on graph convolutional network,” *Applied Energy*, vol. 307, p. 118231, 2022. [Online]. Available: <https://www.sciencedirect.com/science/article/pii/S0306261921014963>
- R. J. Hyndman and S. Fan, “Density forecasting for long-term peak electricity demand,” *IEEE Transactions on Power Systems*, vol. 25, no. 2, pp. 1142–1153, 2010.
- N. Amjady, “Short-term hourly load forecasting using time-series modeling with peak load estimation capability,” *IEEE Transactions on Power Systems*, vol. 16, no. 4, pp. 798–805, 2001.
- K.-B. Song, Y.-S. Baek, D. H. Hong, and G. Jang, “Short-term load forecasting for the holidays using fuzzy linear regression method,” *IEEE Transactions on Power Systems*, vol. 20, no. 1, pp. 96–101, 2005.



- J. W. Taylor and P. E. McSharry, "Short-term load forecasting methods: An evaluation based on european data," *IEEE Transactions on Power Systems*, vol. 22, no. 4, pp. 2213–2219, 2007.
- J. W. Taylor, "An evaluation of methods for very short-term load forecasting using minute-by-minute british data," *International Journal of Forecasting*, vol. 24, no. 4, pp. 645–658, 2008. [Online]. Available: <https://www.sciencedirect.com/science/article/pii/S0169207008000708>
- S. Fan and R. J. Hyndman, "Short-term load forecasting based on a semi-parametric additive model," *IEEE Transactions on Power Systems*, vol. 27, no. 1, pp. 134–141, 2012.
- N. Charlton and C. Singleton, "A refined parametric model for short term load forecasting," *International Journal of Forecasting*, vol. 30, no. 2, pp. 364–368, 2014. [Online]. Available: <https://www.sciencedirect.com/science/article/pii/S0169207013000794>
- Y. Goude, R. Nedellec, and N. Kong, "Local short and middle term electricity load forecasting with semi-parametric additive models," *IEEE Transactions on Smart Grid*, vol. 5, no. 1, pp. 440–446, 2014.
- R. Weron, *Modeling and Forecasting Electricity Loads*. John Wiley & Sons, Ltd, 2006, ch. 3, pp. 67–100. [Online]. Available: <https://onlinelibrary.wiley.com/doi/abs/10.1002/9781118673362.ch3>
- S. Pappas, L. Ekonomou, P. Karampelas, D. Karamousantas, S. Katsikas, G. Chatzarakis, and P. Skafidas, "Electricity demand load forecasting of the hellenic power system using an arma model," *Electric Power Systems Research*, vol. 80, no. 3, pp. 256–264, 2010. [Online]. Available: <https://www.sciencedirect.com/science/article/pii/S0378779609002107>
- E. Chodakowska, J. Nazarko, and L. Nazarko, "Arima models in electrical load forecasting and their robustness to noise," *Energies*, vol. 14, no. 23, 2021. [Online]. Available: <https://www.mdpi.com/1996-1073/14/23/7952>
- G. Dudek, "Short-term load forecasting using random forests," in *Intelligent Systems'2014*. Springer International Publishing, 2015, pp. 821–828.
- Y. Chen, P. Xu, Y. Chu, W. Li, Y. Wu, L. Ni, Y. Bao, and K. Wang, "Short-term electrical load forecasting using the support vector regression (svr) model to calculate the demand response baseline for office buildings," *Applied Energy*, vol. 195, pp. 659–670, 2017. [Online]. Available: <https://www.sciencedirect.com/science/article/pii/S0306261917302581>
- B. Patnaik, M. Mishra, R. C. Bansal, and R. K. Jena, "Modwt-xgboost based smart energy solution for fault detection and classification in a smart microgrid," *Applied Energy*, vol. 285, p. 116457, 2021. [Online]. Available: <https://www.sciencedirect.com/science/article/pii/S0306261921000246>
- M. Shepero, D. van der Meer, J. Munkhammar, and J. Widén, "Residential probabilistic load forecasting: A method using gaussian process designed for electric load data," *Applied Energy*, vol. 218, pp. 159–172, 2018. [Online]. Available: <https://www.sciencedirect.com/science/article/pii/S030626191830299X>
- R. Efendi, Z. Ismail, and M. M. Deris, "A new linguistic out-sample approach of fuzzy time series for daily forecasting of malaysian electricity load demand," *Applied Soft Computing*, vol. 28, pp. 422–430, 2015. [Online]. Available: <https://www.sciencedirect.com/science/article/pii/S1568494614006073>
- C. Deb, F. Zhang, J. Yang, S. E. Lee, and K. W. Shah, "A review on time series forecasting techniques for building energy consumption," *Renewable and Sustainable Energy Reviews*, vol. 74, pp. 902–924, 2017. [Online]. Available: <https://www.sciencedirect.com/science/article/pii/S1364032117303155>
- F. M. Bianchi, E. Maiorino, M. C. Kampffmeyer, A. Rizzi, and R. Jenssen, *Recurrent Neural Networks for Short-Term Load Forecasting*. Springer, 2017.
- I. K. Nti, M. Teimeh, O. Nyarko-Boateng, and A. F. Adekoya, "Electricity load forecasting: a systematic review," *Journal of Electrical Systems and Information Technology*, vol. 7, no. 1, p. 13, 2020. [Online]. Available: <https://doi.org/10.1186/s43067-020-00021-8>

- B.-J. Chen, M.-W. Chang, and C.-J. Lin, "Load forecasting using support vector machines: a study on eunite competition 2001," *IEEE Transactions on Power Systems*, vol. 19, no. 4, pp. 1821–1830, 2004.
- G. Tsekouras, N. Hatziaargyriou, and E. Dyalynas, "An optimized adaptive neural network for annual midterm energy forecasting," *IEEE Transactions on Power Systems*, vol. 21, no. 1, pp. 385–391, 2006.
- A. Sözen, Z. Gülseven, and E. Arcaklioglu, "Forecasting based on sectoral energy consumption of ghgs in turkey and mitigation policies," *Energy Policy*, vol. 35, no. 12, pp. 6491–6505, 2007. [Online]. Available: <https://www.sciencedirect.com/science/article/pii/S0301421507003722>
- Z. W. Geem and W. E. Roper, "Energy demand estimation of south korea using artificial neural network," *Energy Policy*, vol. 37, no. 10, pp. 4049–4054, 2009. [Online]. Available: <https://www.sciencedirect.com/science/article/pii/S0301421509003218>
- F. Ardakani and M. Ardehali, "Long-term electrical energy consumption forecasting for developing and developed economies based on different optimized models and historical data types," *Energy*, vol. 65, pp. 452–461, 2014. [Online]. Available: <https://www.sciencedirect.com/science/article/pii/S0360544213010888>
- G. M. U. Din and A. K. Marnerides, "Short term power load forecasting using deep neural networks," in *2017 International Conference on Computing, Networking and Communications (ICNC)*, 2017, pp. 594–598.
- M. Voß, C. Bender-Saebelkampff, and S. Albayrak, "Residential short-term load forecasting using convolutional neural networks," in *2018 IEEE International Conference on Communications, Control, and Computing Technologies for Smart Grids (SmartGridComm)*, 2018, pp. 1–6.
- D. L. Marino, K. Amarasinghe, and M. Manic, "Building energy load forecasting using deep neural networks," in *IECON 2016 - 42nd Annual Conference of the IEEE Industrial Electronics Society*, 2016, pp. 7046–7051.
- W. Kong, Z. Y. Dong, Y. Jia, D. J. Hill, Y. Xu, and Y. Zhang, "Short-term residential load forecasting based on lstm recurrent neural network," *IEEE Transactions on Smart Grid*, vol. 10, no. 1, pp. 841–851, 2019.
- H. Shi, M. Xu, and R. Li, "Deep learning for household load forecasting—a novel pooling deep rnn," *IEEE Transactions on Smart Grid*, vol. 9, no. 5, pp. 5271–5280, 2018.
- J. Zhang, Y.-M. Wei, D. Li, Z. Tan, and J. Zhou, "Short term electricity load forecasting using a hybrid model," *Energy*, vol. 158, pp. 774–781, 2018. [Online]. Available: <https://www.sciencedirect.com/science/article/pii/S036054421831065X>
- M. Afrasiabi, M. Mohammadi, M. Rastegar, L. Stankovic, S. Afrasiabi, and M. Khazaei, "Deep-based conditional probability density function forecasting of residential loads," *IEEE Transactions on Smart Grid*, vol. 11, no. 4, pp. 3646–3657, 2020.
- G. Dudek and P. Pelka, "Pattern similarity-based machine learning methods for mid-term load forecasting: A comparative study," *Applied Soft Computing*, vol. 104, p. 107223, 2021. [Online]. Available: <https://www.sciencedirect.com/science/article/pii/S1568494621001460>
- L. Yin, X. Cao, and D. Liu, "Weighted fully-connected regression networks for one-day-ahead hourly photovoltaic power forecasting," *Applied Energy*, vol. 332, p. 120527, 2023. [Online]. Available: <https://www.sciencedirect.com/science/article/pii/S0306261922017846>
- S. L. Brunton, J. L. Proctor, and J. N. Kutz, "Discovering governing equations from data by sparse identification of nonlinear dynamical systems," *Proceedings of the National Academy of Sciences*, vol. 113, no. 15, pp. 3932–3937, 2016.
- S. L. Brunton and J. N. Kutz, *Data-Driven Science and Engineering: Machine Learning, Dynamical Systems, and Control*. Cambridge University Press, 2019.

- , “Targeted use of deep learning for physics and engineering,” in *Knowledge-Guided Machine Learning*. Chapman and Hall/CRC, 2022, pp. 31–54.
- K. R. Moon, D. van Dijk, Z. Wang, S. Gigante, D. B. Burkhardt, W. S. Chen, K. Yim, A. v. d. Elzen, M. J. Hirn, R. R. Coifman, N. B. Ivanova, G. Wolf, and S. Krishnaswamy, “Visualizing structure and transitions in high-dimensional biological data,” *Nature Biotechnology*, vol. 37, no. 12, pp. 1482–1492, 2019. [Online]. Available: <https://doi.org/10.1038/s41587-019-0336-3>
- A. M. Tartakovsky and R. Tipireddy, “Physics-informed machine learning method for forecasting and uncertainty quantification of partially observed and unobserved states in power grids,” in *52nd Hawaii International Conference on System Sciences, HICSS 2019, Grand Wailea, Maui, Hawaii, USA, January 8-11, 2019*, T. Bui, Ed. ScholarSpace / AIS Electronic Library (AISeL), 2019, pp. 1–7. [Online]. Available: <http://hdl.handle.net/10125/59779>
- S. Stock, J. Stiasny, D. Babazadeh, C. Becker, and S. Chatzivasileiadis, “Bayesian physics-informed neural networks for robust system identification of power systems,” *arXiv:2212.11911v1*, pp. 1–6, 2022. [Online]. Available: <https://arxiv.org/pdf/2212.11911.pdf>
- I. Mezić, “Spectral properties of dynamical systems, model reduction and decompositions,” *Nonlinear Dynamics*, vol. 41, p. 309–325, 2005.
- H. Lange, S. L. Brunton, and J. N. Kutz, “From fourier to koopman: Spectral methods for long-term time series prediction,” *Journal of Machine Learning Research*, vol. 22, no. 41, pp. 1–38, 2021. [Online]. Available: <http://jmlr.org/papers/v22/20-406.html>
- D. Giannakis, “Data-driven spectral decomposition and forecasting of ergodic dynamical systems,” *Applied and Computational Harmonic Analysis*, vol. 47, no. 2, pp. 338–396, 2019.
- N. Marrouch, J. Slawinska, D. Giannakis, and H. L. Read, “Data-driven koopman operator approach for computational neuroscience,” *Annals of Mathematics and Artificial Intelligence*, vol. 88, no. 11, pp. 1155–1173, 2020.
- G. Froyland, D. Giannakis, B. R. Lintner, M. Pike, and J. Slawinska, “Spectral analysis of climate dynamics with operator-theoretic approaches,” *Nature Communications*, vol. 12, no. 1, p. 6570, 2021.
- J. H. Tu, C. W. Rowley, D. M. Luchtenburg, S. L. Brunton, and J. N. Kutz, “On dynamic mode decomposition: Theory and applications,” *Journal of Computational Dynamics*, vol. 1, no. 2, pp. 391–421, 2014.
- M. O. Williams, I. G. Kevrekidis, and C. W. Rowley, “A data-driven approximation of the koopman operator: Extending dynamic mode decomposition,” *Journal of Nonlinear Science*, vol. 25, p. 1307–1346, 2015.
- K. Fujii and Y. Kawahara, “Dynamic mode decomposition in vector-valued reproducing kernel hilbert spaces for extracting dynamical structure among observables,” *Neural Networks*, vol. 117, pp. 4–103, 2019.
- H. Arbabi and I. Mezić, “Ergodic theory, dynamic mode decomposition, and computation of spectral properties of the koopman operator,” *SIAM Journal on Applied Dynamical Systems*, vol. 16, no. 4, pp. 2096–2126, 2017.
- M. Korda, M. Putinar, and I. Mezić, “Data-driven spectral analysis of the koopman operator,” *Applied and Computational Harmonic Analysis*, vol. 48, no. 2, pp. 599–629, 2020.
- E. H. Thiede, D. Giannakis, A. R. Dinner, and J. Weare, “Galerkin approximation of dynamical quantities using trajectory data,” *The Journal of Chemical Physics*, vol. 150, no. 24, p. 244111, 2019.
- B. Lusch, J. Kutz, and S. Brunton, “Deep learning for universal linear embeddings of nonlinear dynamics,” *Nature Communications*, vol. 9, p. 4950, 2018.
- S. Das and D. Giannakis, “Delay-coordinate maps and the spectra of koopman operators,” *Journal of Statistical Physics*, vol. 175, no. 6, pp. 1107–1145, 2019.

- S. Klus, I. Schuster, and K. Muandet, “Eigendecompositions of transfer operators in reproducing kernel hilbert spaces,” *Journal of Nonlinear Science*, vol. 30, no. 1, pp. 283–315, 2020. [Online]. Available: <https://doi.org/10.1007/s00332-019-09574-z>
- S. Das, D. Giannakis, and J. Slawinska, “Reproducing kernel hilbert space compactification of unitary evolution groups,” *Applied and Computational Harmonic Analysis*, vol. 54, pp. 75–136, 2021.
- R. R. Coifman and S. Lafon, “Diffusion maps,” *Applied and Computational Harmonic Analysis*, vol. 21, no. 1, pp. 5–30, 2006. [Online]. Available: <https://www.sciencedirect.com/science/article/pii/S1063520306000546>
- D. Giannakis and A. J. Majda, “Nonlinear laplacian spectral analysis for time series with intermittency and low-frequency variability,” *PNAS*, vol. 109, no. 7, p. 2222–2227, 2012.
- , “Nonlinear laplacian spectral analysis: capturing intermittent and low-frequency spatiotemporal patterns in high-dimensional data,” *Statistical Analysis and Data Mining*, vol. 6, no. 3, p. 180–194, 2013.
- C. W. Rowley, I. Mezić, S. Bagheri, P. Schlatter, and D. S. Henningson, “Spectral analysis of nonlinear flows,” *Journal of Fluid Mechanics*, vol. 641, p. 115–127, 2009.
- P. J. Schmid, “Dynamic mode decomposition of numerical and experimental data,” *Journal of Fluid Mechanics*, vol. 656, p. 5–28, 2010.
- N. Mohan, K. Soman, and S. Sachin Kumar, “A data-driven strategy for short-term electric load forecasting using dynamic mode decomposition model,” *Applied Energy*, vol. 232, pp. 229–244, 2018. [Online]. Available: <https://www.sciencedirect.com/science/article/pii/S0306261918315009>
- X. Kong, C. Li, C. Wang, Y. Zhang, and J. Zhang, “Short-term electrical load forecasting based on error correction using dynamic mode decomposition,” *Applied Energy*, vol. 261, p. 114368, 2020. [Online]. Available: <https://www.sciencedirect.com/science/article/pii/S0306261919320550>
- D. Dylewsky, D. Barajas-Solano, T. Ma, A. M. Tartakovsky, and J. N. Kutz, “Stochastically forced ensemble dynamic mode decomposition for forecasting and analysis of near-periodic systems,” *IEEE Access*, vol. 10, pp. 33 440–33 448, 2022.
- P. J. Schmid, “Dynamic mode decomposition and its variants,” *Annual Review of Fluid Mechanics*, vol. 54, no. 1, pp. 225–254, 2022. [Online]. Available: <https://doi.org/10.1146/annurev-fluid-030121-015835>
- S. L. Brunton, M. Budišić, E. Kaiser, and J. N. Kutz, “Modern koopman theory for dynamical systems,” *SIAM Review*, vol. 64, no. 2, pp. 229–340, 2022. [Online]. Available: <https://doi.org/10.1137/21M1401243>
- J. Mikkola and P. D. Lund, “Models for generating place and time dependent urban energy demand profiles,” *Applied Energy*, vol. 130, pp. 256–264, 2014. [Online]. Available: <https://www.sciencedirect.com/science/article/pii/S0306261914005340>
- S. Eggimann, J. W. Hall, and N. Eyre, “A high-resolution spatio-temporal energy demand simulation to explore the potential of heating demand side management with large-scale heat pump diffusion,” *Applied Energy*, vol. 236, pp. 997–1010, 2019. [Online]. Available: <https://www.sciencedirect.com/science/article/pii/S0306261918318725>
- J. Peng, A. Kimmig, Z. Niu, J. Wang, X. Liu, and J. Ovtcharova, “A flexible potential-flow model based high resolution spatiotemporal energy demand forecasting framework,” *Applied Energy*, vol. 299, p. 117321, 2021. [Online]. Available: <https://www.sciencedirect.com/science/article/pii/S0306261921007315>
- H. Zhu, Y. Zhu, H. Wang, S. Wang, Z. Liu, B. Balamurugan, P. Vijayakumar, and M. Xia, “Multiscale deep network based multistep prediction of high-dimensional time series from power transmission systems,” *Transactions on Emerging Telecommunications Technologies*, vol. 33, no. 3, p. e3890, 2022. [Online]. Available: <https://onlinelibrary.wiley.com/doi/abs/10.1002/ett.3890>

- S. Das, S. Mustavee, S. Agarwal, and S. Hasan, “Koopman-theoretic modeling of quasiperiodically driven systems: Example of signalized traffic corridor,” *IEEE Transactions on Systems, Man, and Cybernetics: Systems*, pp. 1–11, 2023.
- Z. Niu, J. Wu, X. Liu, L. Huang, and P. S. Nielsen, “Understanding energy demand behaviors through spatio-temporal smart meter data analysis,” *Energy*, vol. 226, p. 120493, 2021. [Online]. Available: <https://www.sciencedirect.com/science/article/pii/S0360544221007428>
- N. Voulis, M. Warnier, and F. M. Brazier, “Understanding spatio-temporal electricity demand at different urban scales: A data-driven approach,” *Applied Energy*, vol. 230, pp. 1157–1171, 2018. [Online]. Available: <https://www.sciencedirect.com/science/article/pii/S0306261918312959>
- T. K. Moon and W. C. Stirling, *Mathematical methods and algorithms for signal processing*. Prentice Hall, 2000.
- L. van der Maaten and G. E. Hinton, “Visualizing data using t-sne,” *Journal of Machine Learning Research*, vol. 9, pp. 2579–2605, 2008.
- T. Berry and J. Harlim, “Variable bandwidth diffusion kernels,” *Applied and Computational Harmonic Analysis*, vol. 40, no. 1, pp. 68–96, 2016. [Online]. Available: <https://www.sciencedirect.com/science/article/pii/S1063520315000020>
- S. Zhong and K.-S. Tam, “Hierarchical classification of load profiles based on their characteristic attributes in frequency domain,” *IEEE Transactions on Power Systems*, vol. 30, no. 5, pp. 2434–2441, 2015.
- R. Li, F. Li, and N. D. Smith, “Load characterization and low-order approximation for smart metering data in the spectral domain,” *IEEE Transactions on Industrial Informatics*, vol. 13, no. 3, pp. 976–984, 2017.
- L. Rydin Gorjão, R. Jumar, H. Maass, V. Hagenmeyer, G. C. Yalcin, J. Kruse, M. Timme, C. Beck, D. Witthaut, and B. Schäfer, “Open database analysis of scaling and spatio-temporal properties of power grid frequencies,” *Nature Communications*, vol. 11, no. 1, p. 6362, 2020. [Online]. Available: <https://doi.org/10.1038/s41467-020-19732-7>
- S. Zhong and K.-S. Tam, “A frequency domain approach to characterize and analyze load profiles,” *IEEE Transactions on Power Systems*, vol. 27, no. 2, pp. 857–865, 2012.
- Y. Yu, H. Jia, P. Li, and J. Su, “Power system instability and chaos,” *Electric Power Systems Research*, vol. 65, no. 3, pp. 187–195, 2003. [Online]. Available: <https://www.sciencedirect.com/science/article/pii/S0378779602002298>
- L. Halekotte, A. Vanselow, and U. Feudel, “Transient chaos enforces uncertainty in the british power grid,” *Journal of Physics: Complexity*, vol. 2, no. 3, p. 035015, jul 2021. [Online]. Available: <https://dx.doi.org/10.1088/2632-072X/ac080f>
- Y. Hu, J. Li, M. Hong, J. Ren, and Y. Man, “Industrial artificial intelligence based energy management system: Integrated framework for electricity load forecasting and fault prediction,” *Energy*, vol. 244, p. 123195, 2022. [Online]. Available: <https://www.sciencedirect.com/science/article/pii/S0360544222000986>
- A. Sharma and S. K. Jain, “A novel seasonal segmentation approach for day-ahead load forecasting,” *Energy*, vol. 257, p. 124752, 2022. [Online]. Available: <https://www.sciencedirect.com/science/article/pii/S0360544222016553>
- T. Hofmann, B. Schölkopf, and A. J. Smola, “Kernel methods in machine learning,” *The Annals of Statistics*, vol. 36, no. 3, pp. 1171 – 1220, 2008. [Online]. Available: <https://doi.org/10.1214/009053607000000677>
- T. Berry and T. Sauer, “Local kernels and the geometric structure of data,” *Applied and Computational Harmonic Analysis*, vol. 40, no. 3, pp. 439–469, 2016. [Online]. Available: <https://www.sciencedirect.com/science/article/pii/S106352031500024X>

- D. Giannakis, “Dynamics-adapted cone kernels,” *SIAM Journal on Applied Dynamical Systems*, vol. 14, no. 2, pp. 556–608, 2015. [Online]. Available: <https://doi.org/10.1137/140954544>
- R. Alexander and D. Giannakis, “Operator-theoretic framework for forecasting nonlinear time series with kernel analog techniques,” *Physica D*, vol. 409, p. 132520, 2020.
- D. Giannakis, A. Kolchinskaya, D. Krasnov, and J. Schumacher, “Koopman analysis of the long-term evolution in a turbulent convection cell,” *Journal of Fluid Mechanics*, vol. 847, p. 735–767, 2018.
- R. R. Coifman and S. Lafon, “Geometric harmonics: A novel tool for multiscale out-of-sample extension of empirical functions,” *Applied and Computational Harmonic Analysis*, vol. 21, no. 1, pp. 31–52, 2006, special Issue: Diffusion Maps and Wavelets. [Online]. Available: <https://www.sciencedirect.com/science/article/pii/S1063520306000522>
- D. Giannakis, “Delay-coordinate maps, coherence, and approximate spectra of evolution operators,” *Research in the Mathematical Sciences*, vol. 8, no. 1, p. 8, 2021.
- T. V. Jensen and P. Pinson, “Re-europe, a large-scale dataset for modeling a highly renewable european electricity system,” *Scientific Data*, vol. 4, no. 1, p. 170175, 2017. [Online]. Available: <https://doi.org/10.1038/sdata.2017.175>
- P. Holmes, J. L. Lumley, and G. Berkooz, *Turbulence, Coherent Structures, Dynamical Systems and Symmetry*, ser. Cambridge Monographs on Mechanics. Cambridge University Press, 1996.
- C. Schlosser and M. Korda, “Sparsity structures for koopman and perron–frobenius operators,” *SIAM Journal on Applied Dynamical Systems*, vol. 21, no. 3, pp. 2187–2214, 2022. [Online]. Available: <https://doi.org/10.1137/21M1466608>
- C. Bishop, *Pattern Recognition and Machine Learning*. Springer-Verlag, 2006.
- A. Tavasoli, T. Henry, and H. Shakeri, “A purely data-driven framework for prediction, optimization, and control of networked processes,” *ISA Transactions*, 2023. [Online]. Available: <https://www.sciencedirect.com/science/article/pii/S0019057823001246>
- R. Mohr, M. Fonoberova, and I. Mezic, “Koopman reduced order modeling with confidence bounds,” *arXiv:2209.13127v1*, pp. 1–32, 2022.
- H. Zhang, C. W. Rowley, E. A. Deem, and L. N. Cattafesta, “Online dynamic mode decomposition for time-varying systems,” *SIAM Journal on Applied Dynamical Systems*, vol. 18, no. 3, pp. 1586–1609, 2019. [Online]. Available: <https://doi.org/10.1137/18M1192329>
- M. Alfatlawi and V. Srivastava, “An incremental approach to online dynamic mode decomposition for time-varying systems with applications to eeg data modeling,” *Journal of Computational Dynamics*, vol. 7, no. 2, pp. 209–241, 2020. [Online]. Available: [/article/id/dcc6e65a-5e68-43cf-812c-1f609975678f](https://doi.org/10.1080/15487717.2020.1811923)
- M. J. Colbrook, L. J. Ayton, and M. Szóke, “Residual dynamic mode decomposition: robust and verified koopmanism,” *Journal of Fluid Mechanics*, vol. 955, p. A21, 2023.